3 Results and discussion

3.1 Studies on ITO

Transparent conducting oxides (TCOs) are materials, widely used for electrodes in photovoltaic (PV) devices [**39**]. Materials with varying properties (conductivity, work function, transparency, etc.) exist [**40**]. It is vital to understand and be able to control these properties, so that the desired functionality in a TCO-based PV device is achieved.

3.1.1 Scanning Electron Microscopy

An important approach in the research of a nano-device like the organic solar cells is to be able to actually "see" into it. Thus its structures and construction can be observed on a nano-scale. This becomes possible by using the so called Scanning Electron Microscope (**SEM**). Its functioning principle can be simplified to shooting focused electrons with defined energy on the surface of an object, collecting the back scattered and secondary ones and visualizing their intensity in a space resolved manner on a monitor. This way one gets a two dimensional monochromatic image, due to the darker-lighter coloring of different conductive spots. The information that is to be seen in a SEM image is the ability of particular spots on the examined surface to give electrons.

Our ITO was examined with SEM. The resulting images are shown on Figure 9 and Figure 10.

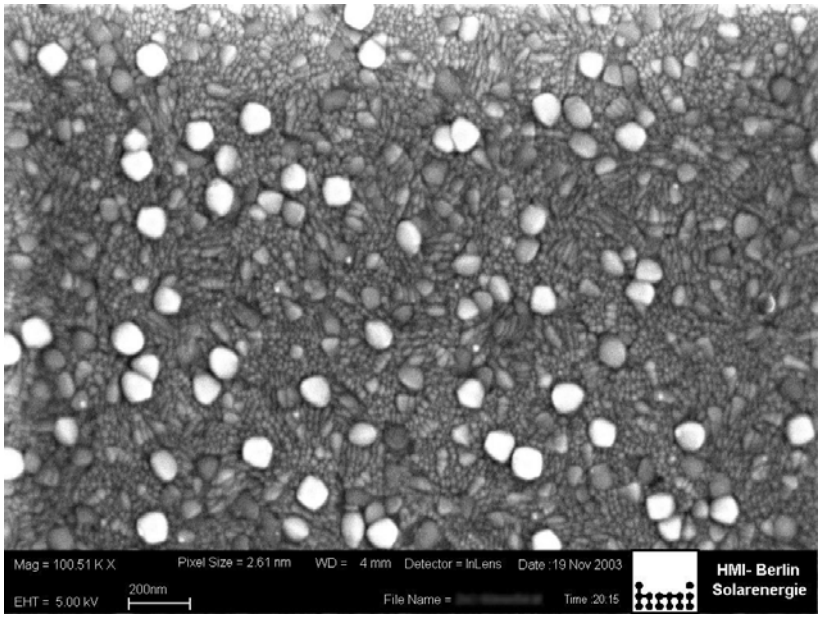

Figure 9. SEM image of our previously used ITO

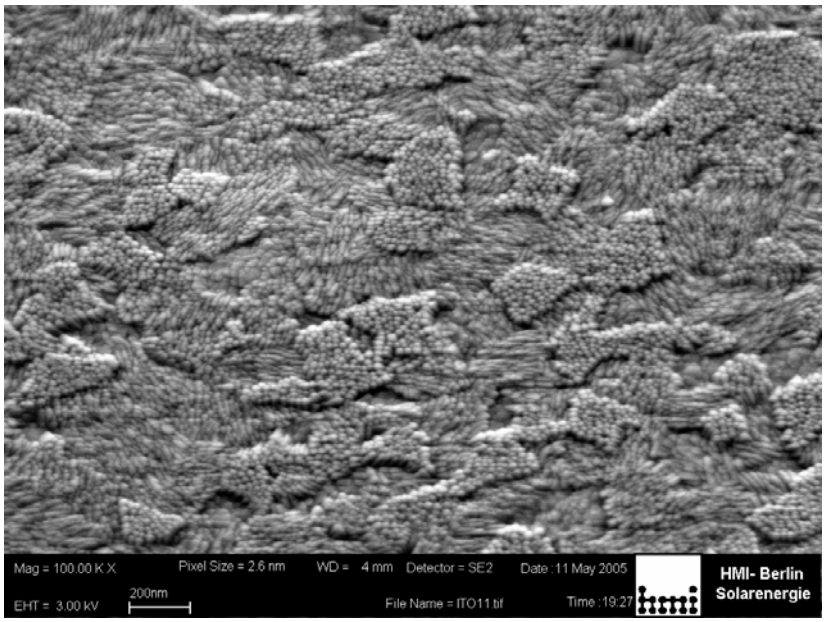

Figure 10. SEM image of our currently used 5 Ω ITO

The ITO shown on Figure 9 is a 10 Ω sample used by us in our early experiments. Here it is shown because an electrodeposition experiment in the current work was conducted exactly on such a sample. This SEM image shows that the majority of the

surface consists of smaller crystallites with size about 10-15 nm, which are relatively flat. There are also bigger islands about 70-100 nm to be seen. Exactly these big crystallites constitute the danger of getting a shortcut through the cell, when the altogether thickness between the contacts is: ZnPc + C60 + BCP = 30 + 30 + 17 = 77 nm. Using PEDOT:PSS, a thick film on the surface is created, thus making it less rough and modifying its work function (more on work function in 0) [**41**]. To avoid working with such rough and inhomogeneous ITO surface we started using another kind of ITO – the 5 Ω (Figure 10). Another reason is of course purely electrical – the lower the electrical resistance of the ITO layer, the higher the currents which can flow. ITO with different resistances will be discussed more detailed in 3.1.2.

The 5 Ω ITO on the contrary has only small crystallites, again about 10-15 nm, organized in bigger 200-300 nm domains. It's roughness as the figure shows is very low and homogeneous.

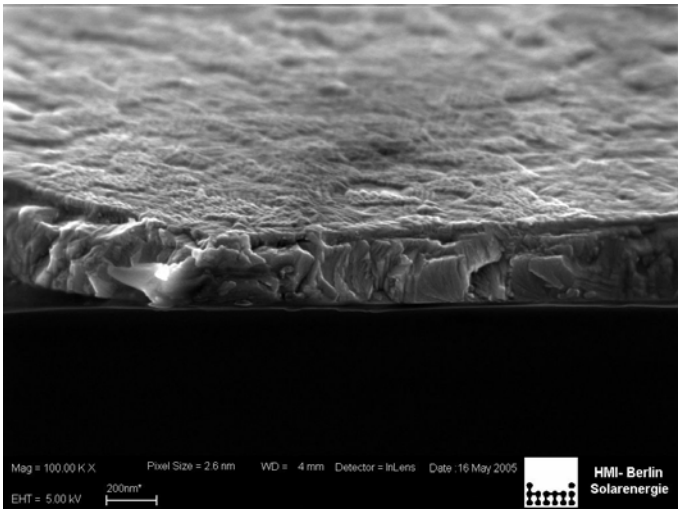

Figure 11. SEM side look at a broken edge of 5 Ω ITO

This morphology allows thinner or even monolayer passivations to be used and still have no shortcuts. A look from the side on a broken edge (Figure 11) of this 5 Ω ITO-glass sample proves this. It also shows the structure of the bulk beneath the surface. It is a homogenous material, without cavities. Interesting is that the grain structure of the surface is not the building block of the volume. On the contrary the bulk has a solid, flake-like structure, possibly due to different, from the surface material, sputtering conditions. The overall ITO thickness of this sample can be roughly estimated, from the image, to about 300 nm.

3.1.2 Different ITO types by resistance

Another parameter of a TCO layer is its sheet resistance. The resistance "R" of a semiconductor rectangular block with resistivity "ρ", length "L" and cross section "A" is given by the formula: $R = \rho.\frac{L}{A}$. If "B" is the width of the sample and "C" is its thickness then $A = B.C$. So the formula for the resistance could be modified: $R = \frac{\rho}{C}.\frac{L}{B}$. The sheet resistance is defined as material resistivity divided to the layer thickness $R_s = \frac{\rho}{C}$. Strictly speaking, the unit for sheet resistance is Ohms (since L/B is unitless), but one refers to it as being in Ohms per square to avoid confusion between R and R_s.

For TCO semiconductor layers with thicknesses less than 0,5 micron the dependence between thickness and sheet resistance is very strong. For example ITO on glass samples from our provider, the company PGO GmbH, had the following properties (Table 2):

ITO type	R_S (statistically measured) [Ω/square]	Typical thickness [nm]
CEC005	4,5	310
CEC007P	6	260
CEC010	8,5	180
CEC020	15	100
CEC030P	24	65
CEC050	40	40
CEC100	80	23
CEC120S	100	21

Table 2. Standard square resistances / ITO film thicknesses (PGO GmbH website) [42]
In the present work mainly CEC005 is used
and only the electro-codeposition study (3.5.3) is done on CEC010 ITO type

So to diminish the R_S by factor 2, one needs to about double the thickness. The problem here comes from the fact that, by increasing the overall thickness of the TCO layer one also increases the quantity of light absorbed in it. For example in four cases for the ITO-types 5s, 10p, 20s, 50s the company PGO GmbH gives the transmissions shown in Figure 12. It is obvious that in direction of increasing the resistance and decreasing the layer thickness the optical absorption also decreases.

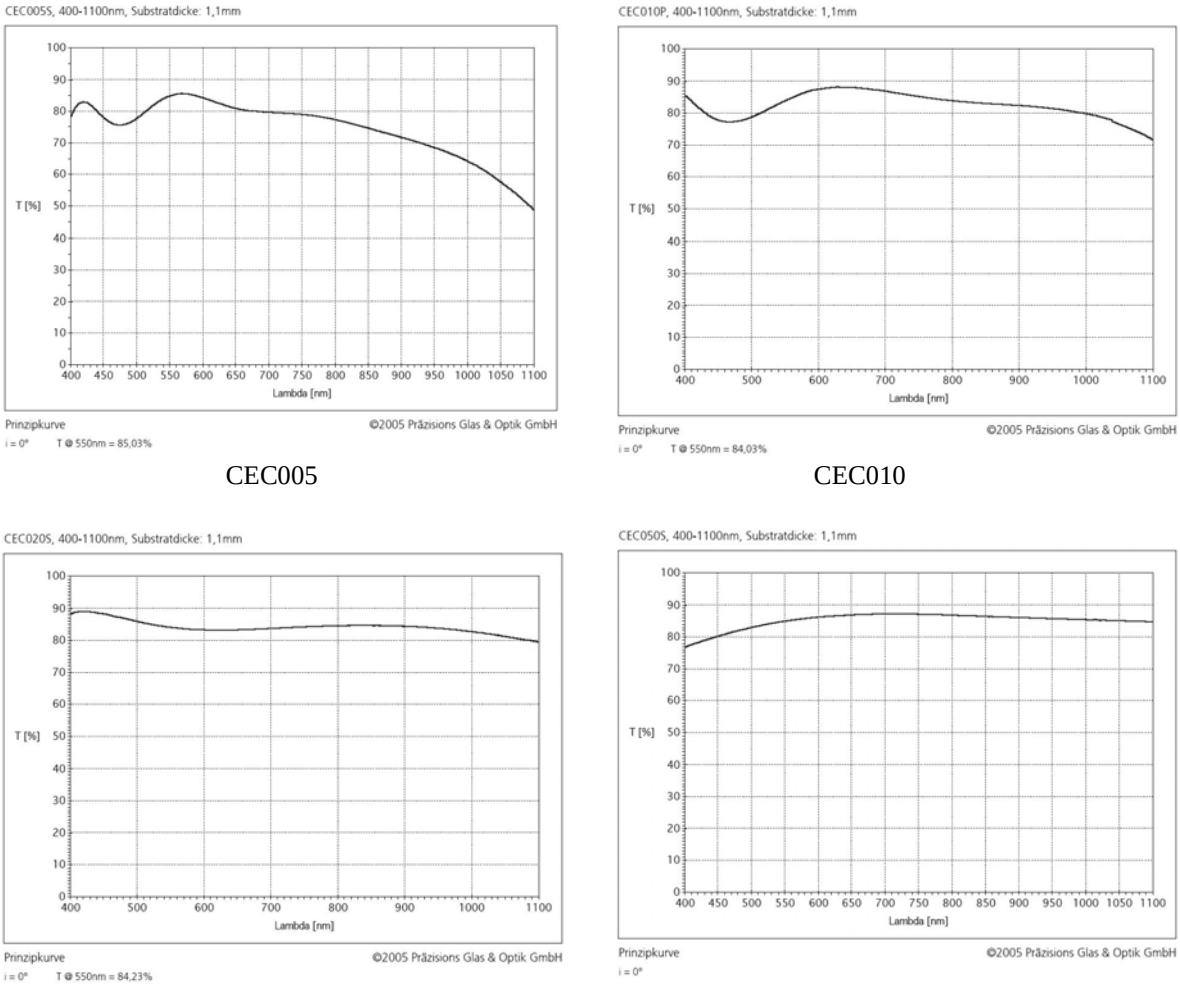

Figure 12. Optical transmissions of 5, 10, 20 and 50 Ω/□ ITO-glasses, ordered by incrementing resistance [42**]**

These four different kinds of ITO we tested in a complete solar cell. Conducting the evaporation of the active layers on these four substrates on the same sample holder assured the same conditions and layer thicknesses for all the cells. The result corresponds to what we expected and is shown on Figure 13.

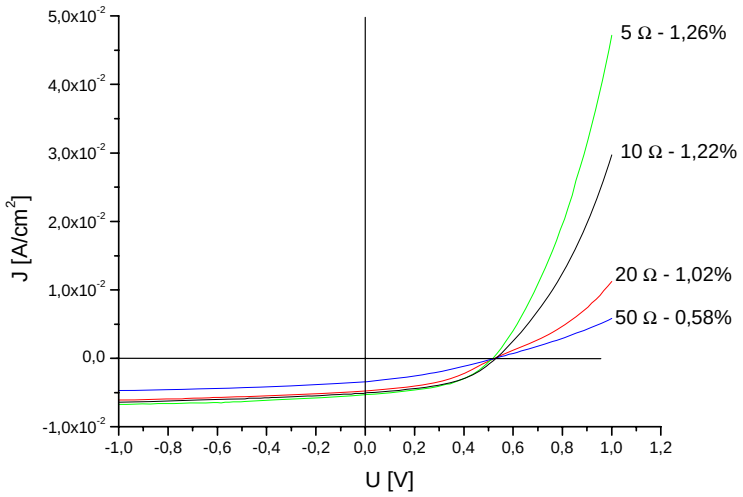

Figure 13. I/V curves of standard cell on ITO substrates with different resistances and their corresponding efficiencies in %

This result clearly shows that the effect on power conversion efficiency from conductivity gain is stronger than that of optical transmission loss.

3.1.3 Annealing/Resistance

Another factor with strong influence on the cell properties is the substrate temperature during the vacuum evaporation of the active layers [**43**]. That is why a temperature test of the TCO substrate was conducted. To see how ITO electrode behaves at higher temperatures, a sample with contacts connected to an ohm-meter, was placed in an oven and heated up to 350°C in steps of 50°C. The plotted graph of resistance vs. temperature, measured in-situ is shown in Figure 14.

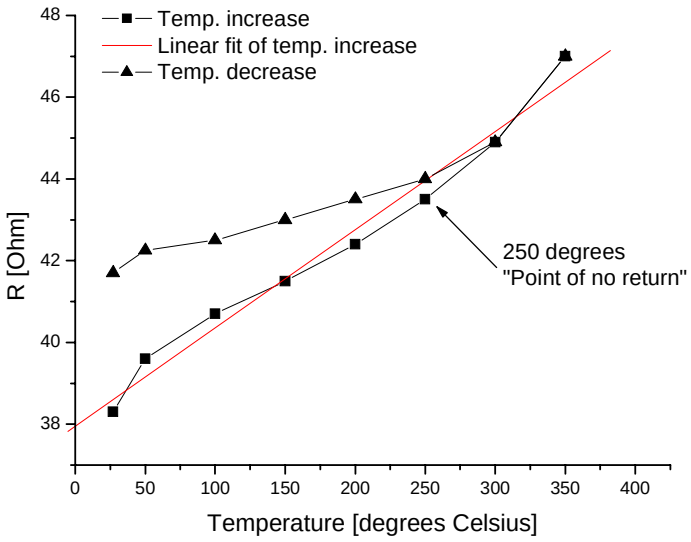

Figure 14. ITO – temperature dependence of its resistance (not sheet resistance)

The dependence of the parameters is almost linear up to 350°C, as expected. Though, the sample can be annealed only up to 250 degrees without making irreversible changes. If annealed to 250 and cooled ITO retains its initial resistance. Heated higher than 250°C there already is some obvious change, which affects the resistance also while cooling (dataset marked with triangles). At the end, already at room temperature the sample has changed and instead of its initial 38,3 Ω it shows 41,7 Ω between the contacts. From this experiment we conclude that the temperature of the substrate should never exceed 250°C [43].

3.1.4 Work function - KPFM, XPS

One of the most important properties of a TCO, which also influences the choice when starting new device architecture, is its surface work function. A crucial point in an organic PV device is the interface between the inorganic TCO and the first organic layer [**44**]. Schottky barrier, bad charge transfer, recombination at defects are some of the problems which might occur. That is why, studying the surface work function is important, if one wants to fit the TCO to the needs of the specific task.

As already mentioned (in 1.3) in the scientific literature there are very different opinions concerning the ITO work function value. We measured it using Kelvin Probe Force Microscopy (KPFM) and X-Ray Photoelectron Spectroscopy (XPS) and the results were in good agreement. KPFM as a method could be simply described as an Atomic Force Microscope (AFM), which can also measure the contact potential of the monitored surface. From the contact potential the work function is calculated using the formula: $\Phi = (4,5 - CP_{CL}) + CP_{Sub}$, where CP_{CL} is the contact potential of the KPFM cantilever and CP_{Sub} is the contact potential of the substrate. The value 4,5 comes from the calibration of the cantilever.

The KPFM image is shown on Figure 15. As standard the sample was heated up to 130°C in high vacuum to remove water adsorbed on the surface and measured after that. If some change in ITO during this heat treatment happened this method cannot tell.

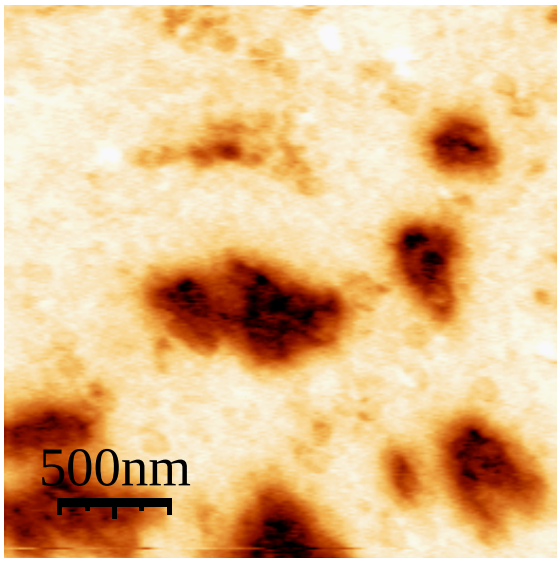

Figure 15. KPFM image of the work function distribution on the clean ITO surface[1]; measured in dark, after annealing in UHV at 130°C, 30min; darker spots indicate lower values, brighter areas – higher values

The minimal value measured is 3,56 eV and the maximal 4,48 eV. The mean work function value is found at 4,3 eV. What one also sees, is that the distribution is very uneven and big spots of low work function areas are present.

The other method for measuring surface work function, namely XPS, determines the value on a bigger scale thus the result is a mean value of the entire measured area. The work function value calculated from the XPS measurement is 4,2, which is in good agreement with the one measured by KPFM. We now assume this value for a clean and untreated ITO in all our further comparisons and diagrams.

[1] Measurement: N. Barreau, HMI

3.2 Active layers stability tests – FTIR

The problem with the degradation of organic photovoltaic devices was already discussed in 1.4. There it was also mentioned that one hypothetical route to degradation is the UV activation of the substance of the active layers, thus allowing diffusing oxygen to chemically destroy them and their initial properties. We studied this possible way of degradation with Fourier Transform Infra-Red spectroscopy (FTIR). Measurements were conducted on a BRUKER FTIR spectrometer.

At first IR spectra of the pure ZnPc and C_{60} in a KBr pill were recorded. Then powder samples of the pure substances were exposed to UV light under a 150 W Xenon-Arc lamp (ORIEL Instruments) for 12 hours. After this the IR spectra in KBr were measured again and compared with the ones before UV exposure. Differences in the spectra, before and after UV treatment, were expected, because of changed chemistry. All substances were exposed to air all the time. The spectrum of BCP was taken basically to be compared with a reference spectrum from literature, to verify if the substance is identical and free from contaminants. The results are shown on the following figures (Figure 16 to Figure 19):

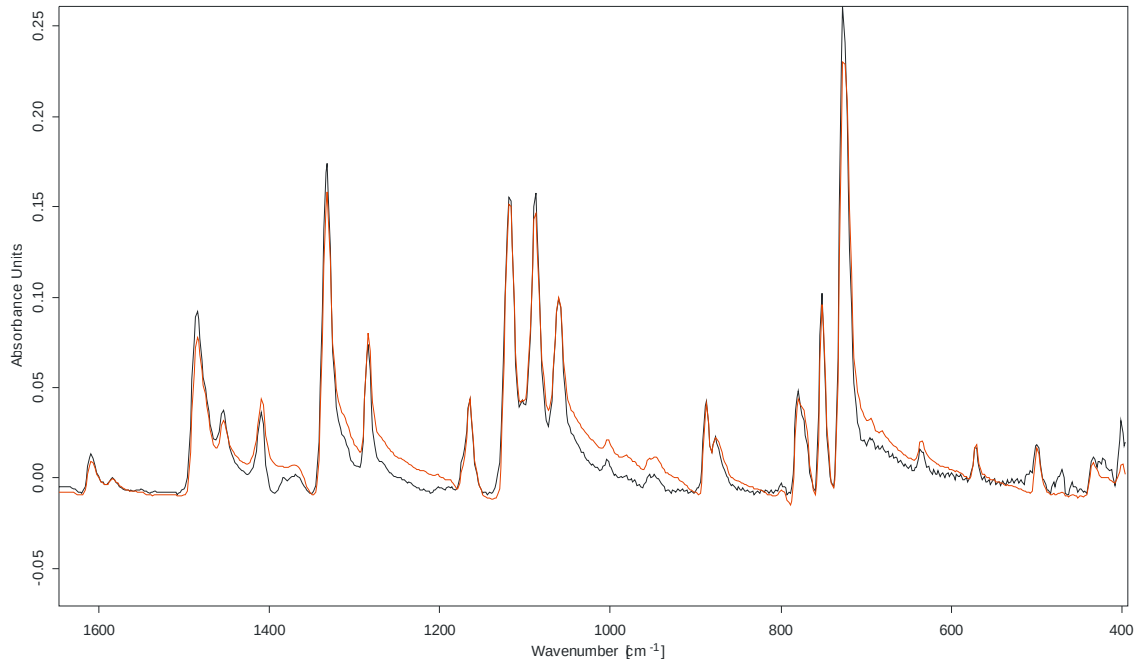

Figure 16. FTIR spectra of ZnPc in KBr before (black) and after (red) 12h UV light treatment of the substance in powder form. Shown is only the fingerprint range. Absorbance of both spectra is normalized for comparison purpose. Differences are observed only in absorbance, but not in peak position. Peak disappearance around 500 cm^{-1} is attributed to compensation problem

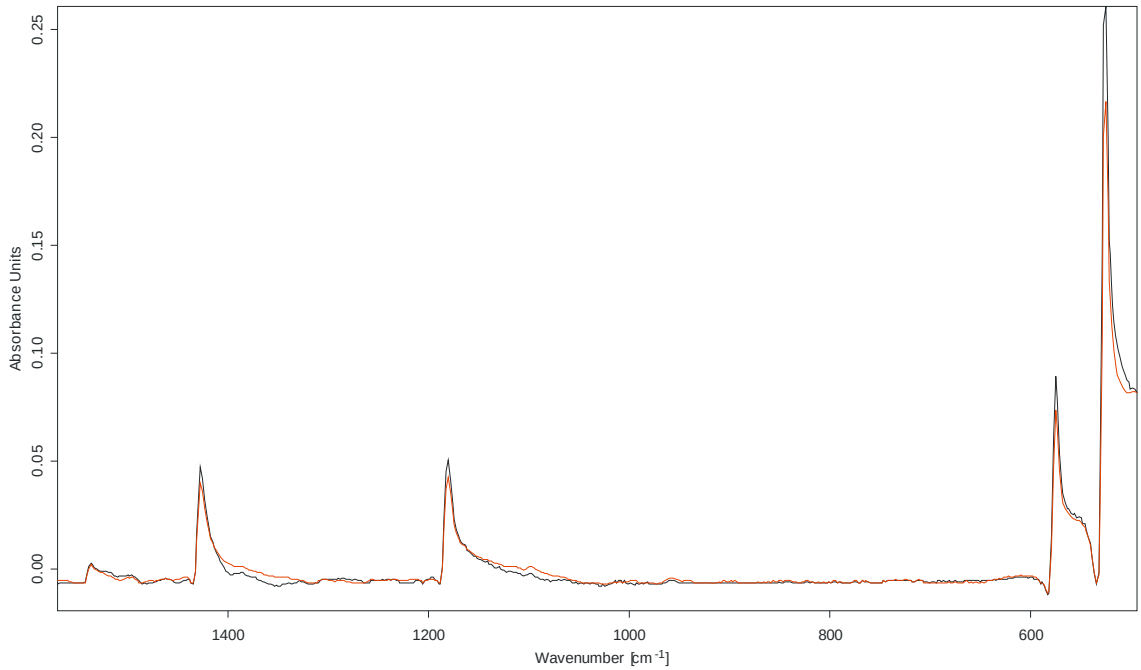

Figure 17. FTIR spectra of C_{60} in KBr before (black) and after (red) 12h UV light treatment of the substance in powder form. Absorbance of both spectra is normalized for comparison purpose. As with ZnPc, differences in C_{60} spectra are observed only in absorbance, but not in peak position or number of peaks. This is a hint for stable chemistry

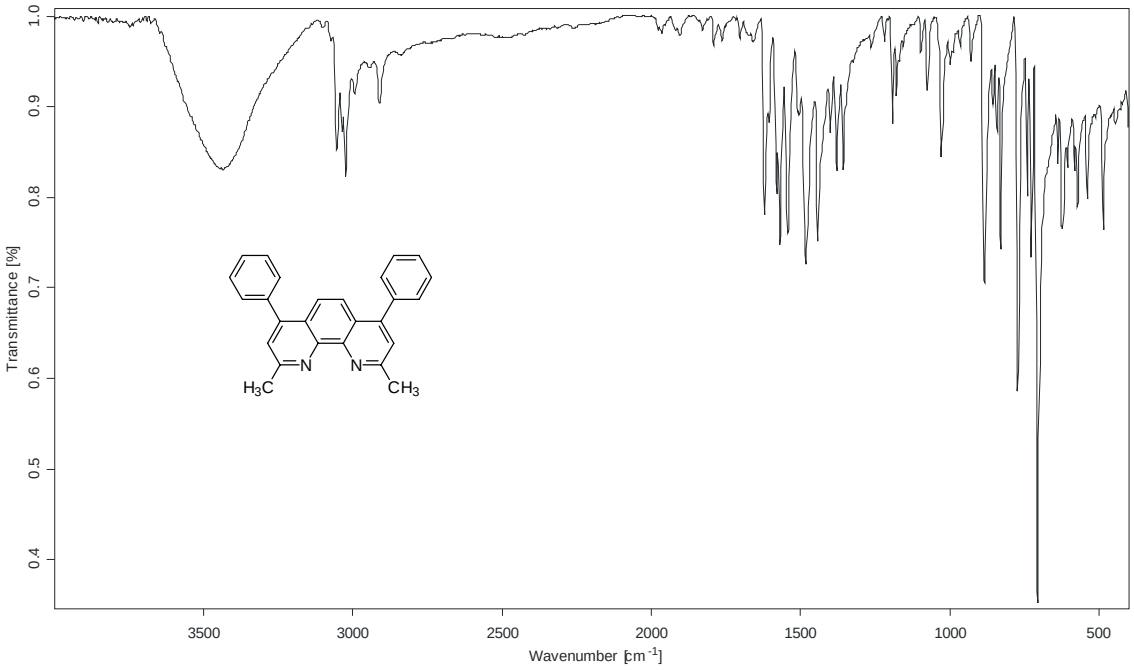

Figure 18. FTIR transmittance Spectrum of BCP in KBr

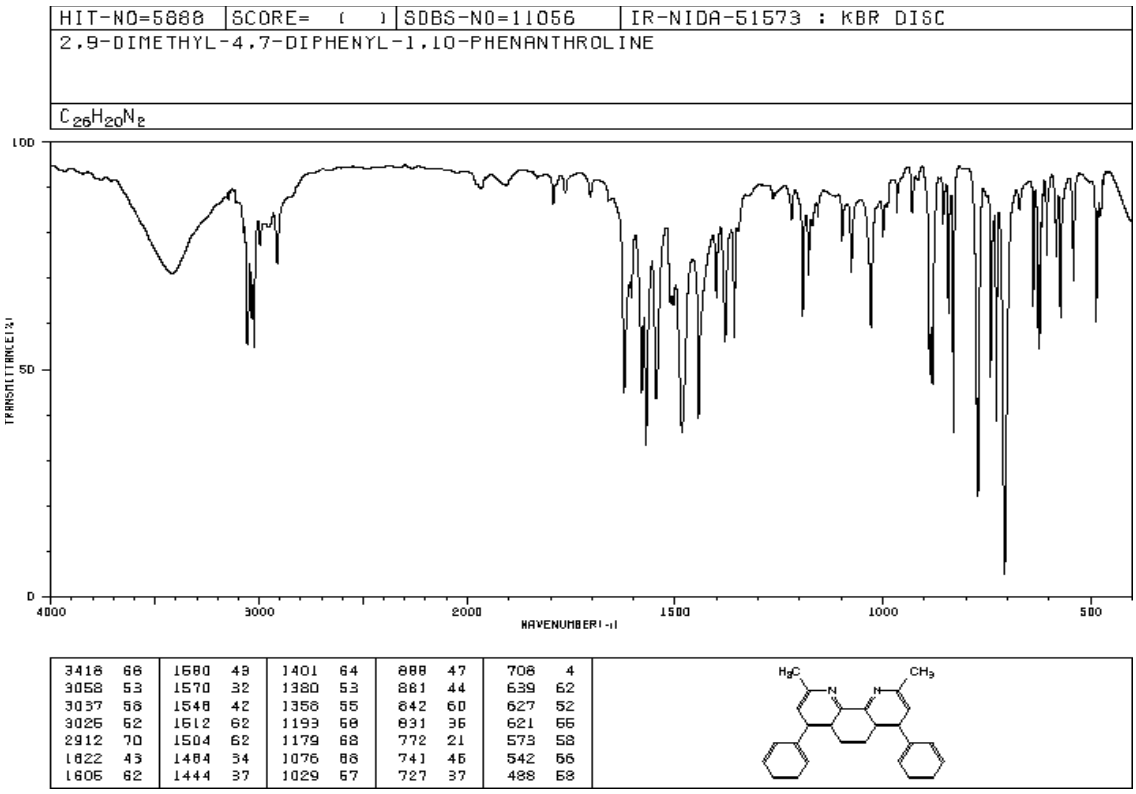

Figure 19. FTIR transmittance spectrum of BCP from Spectral Database for Organic Compounds SDBS; x-axis has two different scales, before and after 2000 cm^{-1}

It is astonishing that on the spectra of both ZnPc and C60, before and after UV light treatment in air, there is no noticeable new peaks to observe. The only dissimilarities between the spectra are compensation problems (water contents in sample, different vacuum quality during measurements). The reason, for these matching spectra, may lie in the fact that the substances were in powder form during the UV treatment. Possibly the chemistry could have changed only on the surface of the powder particles. This would be a very small quantity of material and its IR signal could be easily suppressed by the peaks of the bulk material. The method sensitivity lies beyond one percent, but since the initial material purity is ca. 99%, it can be concluded that no additional impurity was detected.

The IR spectrum of BCP is in good agreement with the reference one from literature.

The material stability shown by this study does not explain the cause of cell degradation. It can only be hypothesized about the degradation background and cause. It is possible that the separate substances show stability, which after bringing them in contact changes. Probably in contact the reaching of thermodynamic equilibrium destabilizes the molecules, thus making them vulnerable to aggressive gas radicals, created by the UV irradiation. The cell degradation in encapsulated state is a suggestion that the radicals could be emitted from the ITO, which is a non-stoichiometric metal oxide and can contain excessive amounts of oxygen.

3.3 UV-VIS Spectroscopy of cell layers and computer simulation

In 1.2 our cell architecture was described, as practically optimized i.e. the thickness of the active layers in the cells was changed, until an optimum in efficiency was reached, using the trial and error principle. This way a good starting efficiency was reached, from where all optimizations of these organic PV devices began.

Although these devices worked fine, a theoretical backbone was somewhat missing. One did not know if the thickness of every layer was really the optimal or whether there could be a better optimized one. That is why a theoretical simulation of this PV device was required. More exactly, the phase distribution of different wavelengths of light in the cell was of interest. That means, where exactly the different wavelengths have their phase maxima in the cell.

A simulation of a multilayer solar cell is a complicated task. It is done by a computer program, where one feeds in data about every single layer's material – its refraction index "**n**" and extinction coefficient "**k**" over the interval of utilizable light wavelengths i.e. 350-850 nm (mostly visible light). **n** and **k** can not be obtained by any direct measurement. They have to be calculated from other spectroscopic data (see **Appendix A** for theoretical basis).

3.3.1 Practical measurement of R and T; n and k calculation

In order to determine the optical constants of Zn-phthalocyanine, C60 and Bathocuproine 50nm layers have been evaporated separately on a quartz substrate. The ITO was already sputtered on a glass substrate. According to the provider, PGO, the ITO had a layer thickness of 180 nm but the value, measured and used by us was 150 nm.

The reflection and transmittance of the samples have been determined with a "Cary 500Scan UV-Vis-NIR Spectrophotometer" in dependence of the wavelength. At first the clean substrate was measured and then the film evaporated on the substrate.

To make the data compatible to the "Optik"-program[2] and perform Kramer-Kronig calculations they must be formatted in a special way. At the beginning the optical constants **n** and **k** for the substrate must be calculated by the program. These constants must be written in a file used for determination of the constants of the thin films. Calculating the n- and k-values of the film follows in a second step.

From our measurements we obtained the data, shown on the following diagrams:

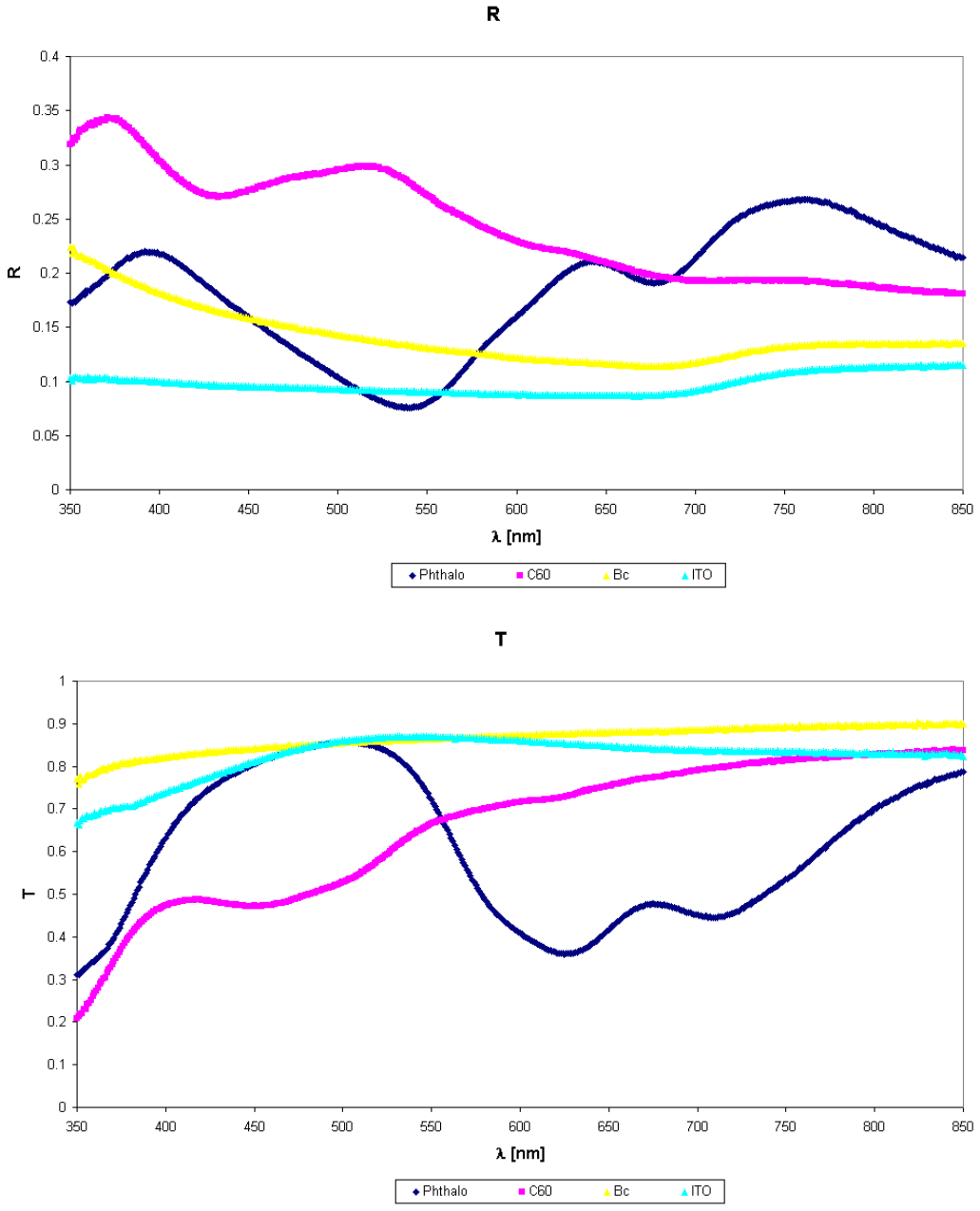

Figure 20. Reflection and transmission data, obtained from the spectroscopic measurements in reflectance (upper plot) and transmission (lower plot) geometry, in absorption units

[2] The program "Optik" is written by Kristian Peter

Calculations with the program “Optik” yielded the following results:

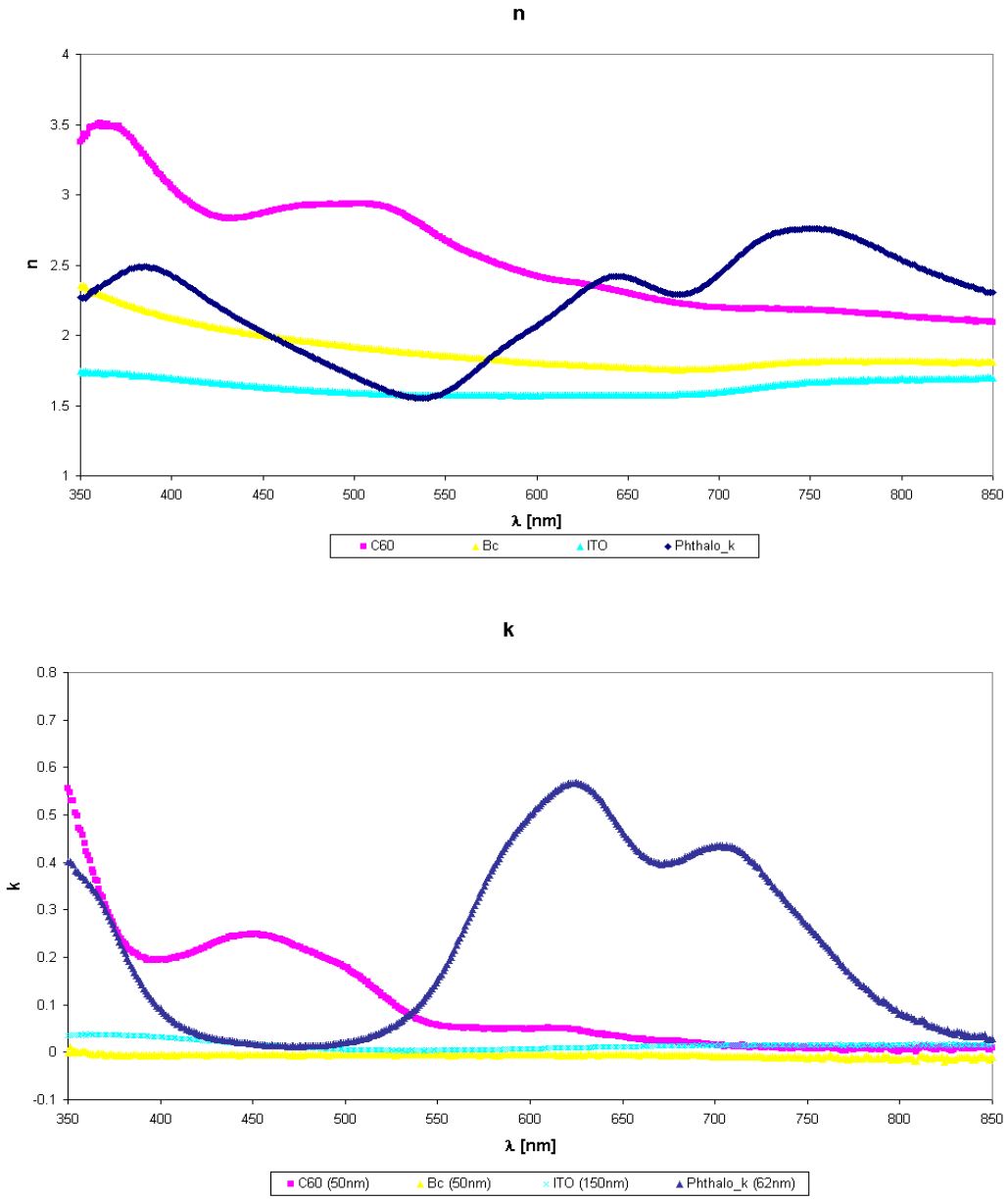

Figure 21. Plots of the calculated (with the “Optik” program) data for refraction index (upper plot) and extinction coefficient (lower plot). The values in brackets show the layer thicknesses evaporated on the substrate, measured with CARY and used for the calculation in the “Optik” program

For application in a solar cell it is especially important to know what optical absorption each material has. The absorption coefficient α is connected with the

extinction coefficient in the following relation: $\alpha = \frac{4\pi k}{\lambda}$. From this relation one can estimate the absorption from the diagram for k.

So in the k/λ diagram it is to observe that C_{60} has a relative absorption maximum at about 450 nm and at wavelengths bigger than 550 nm there is almost no absorption. ZnPc has two characteristic absorption maxima. One is around 625 nm and the second, not so intensive just above 700 nm. The absorptions of Bathocuproine and ITO are, as desired, very low. This way the absorption of the solar cell consists mainly of the absorption sum of the active layers ZnPc and C_{60} which almost do not overlap, but complement each other (see Figure 21; pink curve stays for C_{60} extinction and dark blue for ZnPc extinction; extinction is proportional to absorption). The combination of these two substances in a solar cell covers a big part of the solar spectrum (shown on Figure 22).

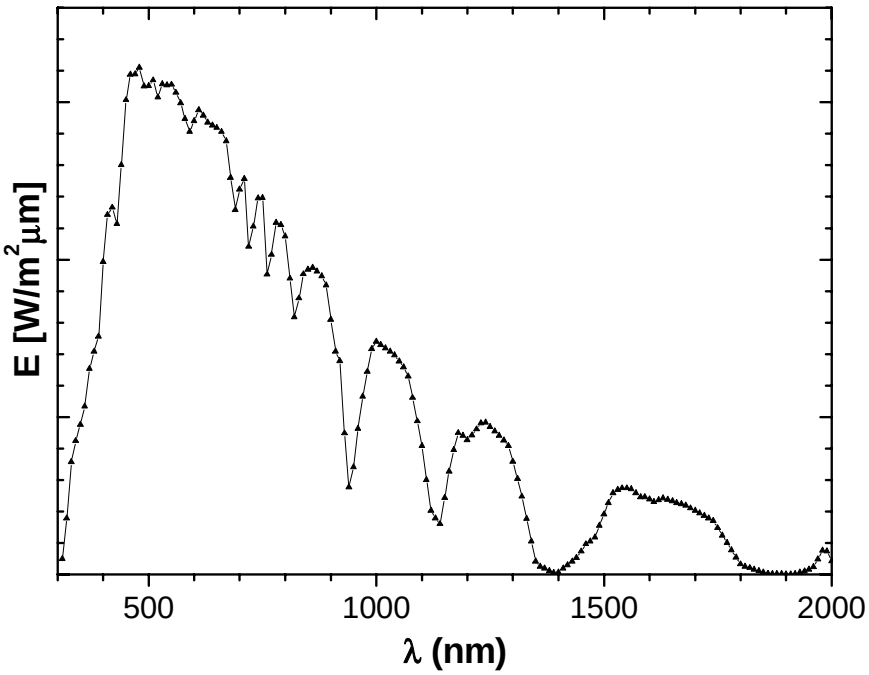

Figure 22. The AM 1.5 G solar energy spectrum [45**].**
Its maximum lies at about 500 nm, where our cell has an absorption gap (above 550 nm)

The maximum of the solar spectrum lies at about 500 nm. There our cell has a gap in absorption. This value is just between the maxima of the absorptions of C_{60} and ZnPc, so there the cell absorbs very weak. There could be a possible improvement in

efficiency, if by any means, by chemical modifications or additional absorber material, the wavelengths around 500 nm are better absorbed.

To estimate the accuracy of our calculations the resulting data was compared with the literature. For ZnPc a comparison with the data obtained by [**46**] in 1992 showed a good agreement between the results.

For C_{60} the result comparison with P. Milani et al. 1994 [**47**] and A. Richter et al. 1995 [**48**] showed a mismatch in the initial layer thickness value given to the "Optik" program for the calculation. A corrected layer thickness value was found, which brought the results to a good agreement with the ones from literature. That is why for the further simulation of the cell, the calculations for C_{60} **n** and **k** were repeated with the corrected layer thickness.

For ITO and Bathocuproine as colorless materials the data on the diagrams are in good agreement with the expected ones.

3.3.2 Optical simulation and result discussion

With the assumption, that our calculations were right and that we had the right datasets for all the layers of our cell, an optical simulation of the distribution of light intensity in our cell was made. This simulation makes sense only for the thin organic solar cells as their overall thickness is less than light wavelength and knowing the distribution of light intensity is an important precondition to their optimal construction. The thicknesses of the separate layers are set to the typical values for our standard cell: ITO – 180 nm; ZnPc – 30 nm; C_{60} – 30 nm; BCP – 17 nm. The result of the optical simulation is a distribution of the electrical field square in the cell. Because of the aluminum electrode, acting as a mirror for the incoming light, for every wavelength a standing wave arises. For all standing waves there is a common knot on the aluminum surface. The resulting distribution is shown on Figure 23:

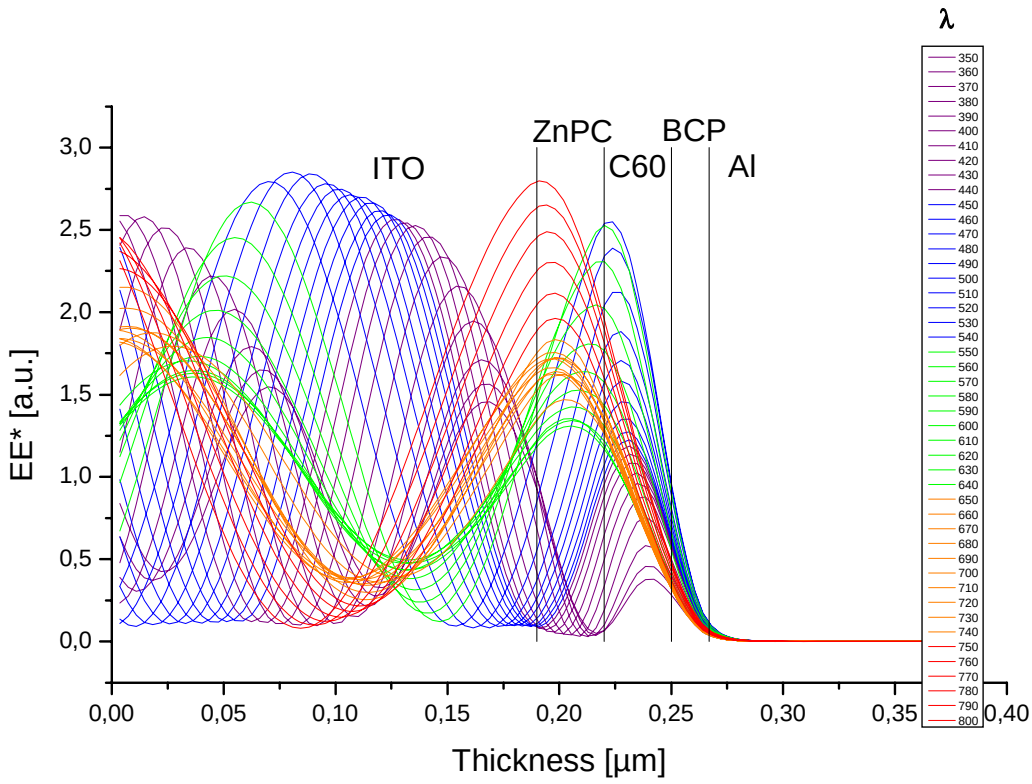

Figure 23. Computer simulated distribution of the electrical field square in the multilayer system ITO/ZnPc/C_{60}/BCP/Al. Color corresponds roughly to wavelength color

For clarity, also a simplified diagram is provided on Figure 24.

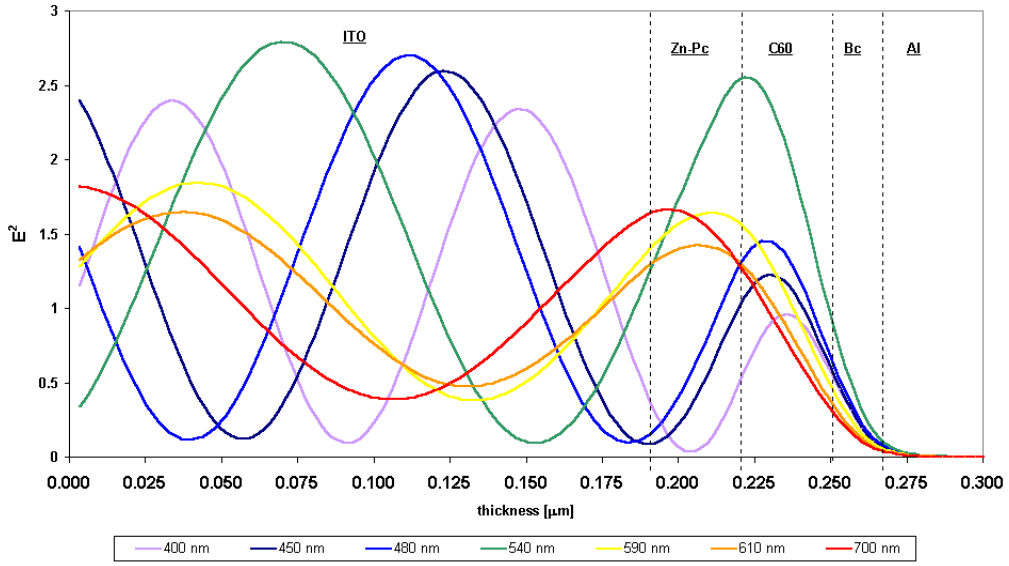

Figure 24. Simplified distribution of the electrical field square [a.u.] in our solar cell. Green light (around 550nm) is almost unabsorbed due to absorption gap in the cell

An important note should be added here, that for the simulation, the interfaces between the material layers in the cell are assumed flat and it is also assumed that no mixing occurs at those interfaces!

The distribution of the square of the electrical field is proportional to the energy density distribution. So from the optical simulation results, the light intensity distribution in the cell can be estimated.

From the graph, it can clearly be seen, that after passing through ITO only a small part of the UV-light is being absorbed. All other wavelengths reach the active layers intact.

The absorption maximum of C_{60} lies at about 450 nm. Apparently the maximum of this wavelength lies aside from the C_{60} layer midpoint. For a full absorption the layer could be made 5-10 nm thicker.

The maxima of ZnPc absorption peaks are ca. 620 nm and 720 nm. The maxima, of the distribution of these wavelengths in the cell, lie displaced from the ZnPc layer middle. For moving these into the middle of the ZnPc layer the thickness of ZnPc can not be increased [14]. Due to the limited charge transport properties of this material (explained in 1.3) this is impossible.

BCP could also not be made thicker, so that the corresponding maxima are set in their right places, because of its insulating properties. In this case a spacer layer is recommended, directly before the aluminum contact, i.e. a layer of a substance which does not absorb in the region 350-800 nm and which is a good electrical conductor.

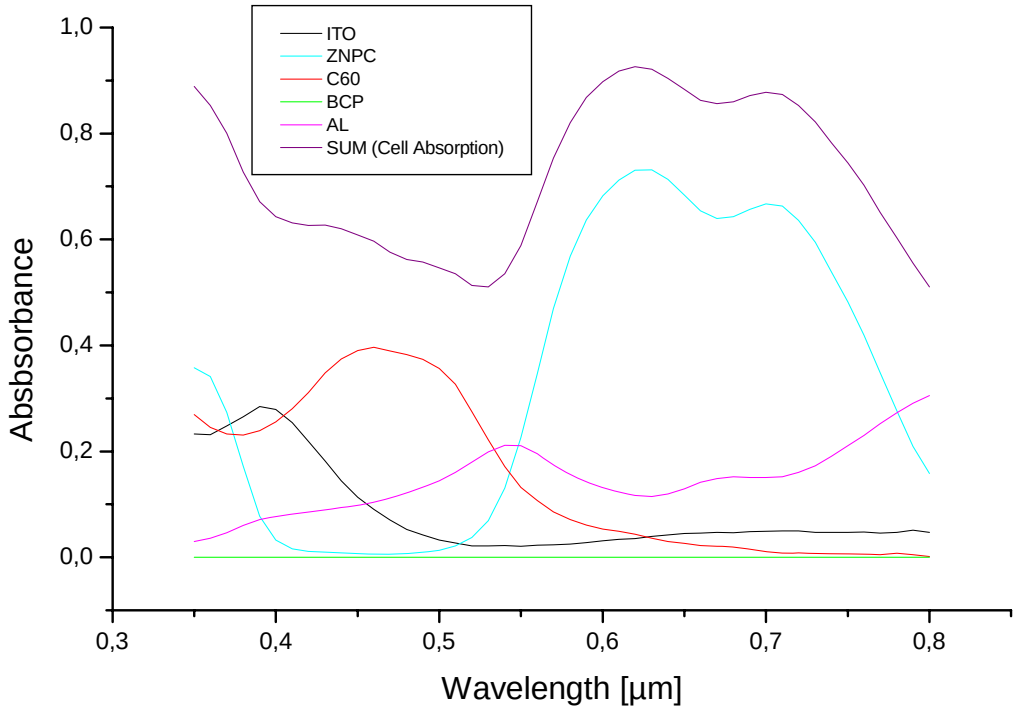

Figure 25. Theoretically calculated absorptions of the different materials in our solar cell, and their sum, the complete cell absorption. The weak absorption in the region around 540 nm does not match the sun spectrum maximum, lying around 500 nm

From the theoretically calculated absorptions (Figure 25) it appears that the wavelengths around 540 nm are absorbed very weak from the active layers. Unfortunately the maximum intensity of the sun spectrum lies at 500 nm. A solution to that would be to extend the cell absorption by either incorporating a second absorber material, absorbing in this region, or by chemically modifying ZnPc in such a way that it covers a wider part of the spectrum.

3.4 Layer thickness measurements

In the previous chapter the importance of exact layer thickness determination was emphasized on for result reproducibility, calculation and/or estimation accuracy. As it was mentioned in 2.7, during the solar cell layer evaporation in UHV, the layer thickness is being monitored by quartz crystal deposition controllers (QCDC), situated next to the rotating ITO substrates. By the producer company Inficon it is claimed, that after correct calibration, these deposition controllers can measure accurate, even tenths of an angstrom deposited layer thickness. It is only required one absolute thickness measurement to calibrate them. But calibration on nanometer scale is not an easy task. As it will be seen further, many different thickness measurement methods had to be employed, and their results compared, in order to accomplish this task.

3.4.1 Profilometer measurement

At first a very fast and easy method was tried – DekTak profilometer. With roughly calibrated deposition controllers, a defined layer thickness of each cell material were deposited on plain glass. Then a sharp scratch with a scalpel, through the layer was inflicted. Thus a step, with sharp edges was created, reaching from the surface of the organics to the glass substrate and having the height of the deposited material. Perpendicular to this scratch, the surface profile was then measured with profilometer. An example of the resulting measurement printout for 200 nm C_{60} layer can be seen on Figure 26.

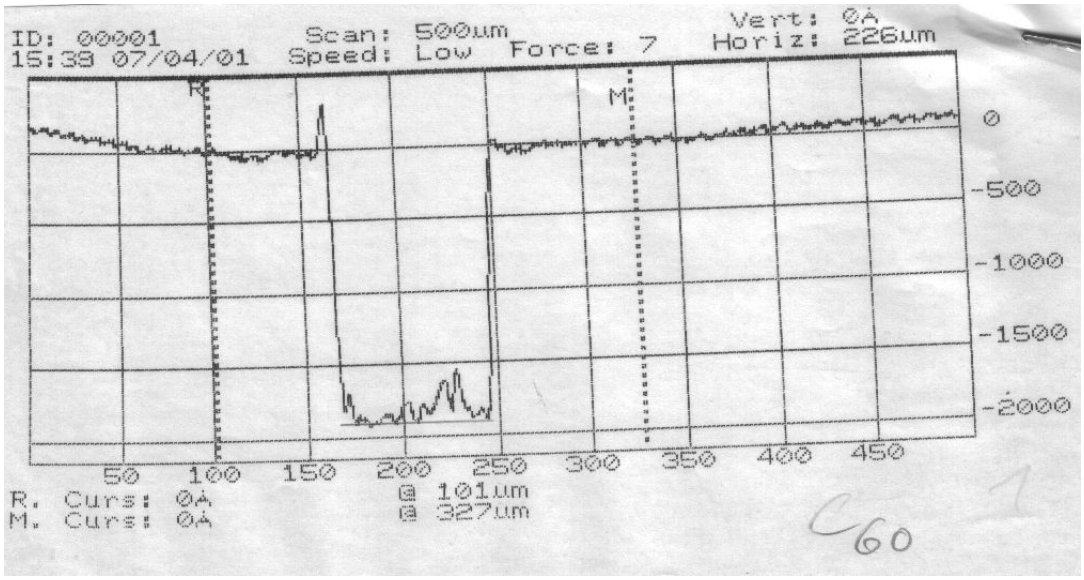

Figure 26. Profilometer printout for a measurement, perpendicular to a scratch in a 200 nm C_{60} layer. Horizontal scale – distance [μm], vertical scale – height (film thickness) [Å]. Method accuracy is not better than 10%, for this thickness scale and soft material surface.

The image shows the profile of a scratch in a 200 nm layer of C_{60}. The mean value of the surface height is set as zero, and the value of the scratch bottom is chosen as layer thickness. From the figure, it is clear how big the error on the nanometer scale can be, having in mind that the bottom of the scratch can never be made flat and even enough to diminish the mistake. Also the soft nature of the organic materials, whose thickness is being measured, allows the cantilever of the profilometer to penetrate the layer, thus additionally distorting the measurement result. So with this, more than 10% error, the method proves as unreliable, but a good approximation, concerning simplicity and low time-consuming measurement.

3.4.2 X-ray reflection[3]

The x-ray reflection provides angstrom exact layer thickness measurements. It requires very flat surfaces and also layers not thicker than 30-40 nm [**49**]. Its principle could be summarized, as Bragg-reflection of x-rays from parallel surfaces – layer and

[3] X-ray reflection measurements conducted by R. Steitz, SF1, HMI

substrate surface, at constantly changing angle. As a result a plot of reflectivity against the angle can be constructed, where the layer thickness can be calculated from the peak position.

For a substrate with low roughness, pre-cut, polished silicon wafers were used (100 Si crystal side). On the substrates 30 nm ZnPc, C60 and BCP were vacuum evaporated. These thicknesses were measured by our quartz crystal deposition controllers. An x-ray reflection measurement of all samples was made. The resulting plot reflectivity/angle for ZnPc is shown on Figure 27.

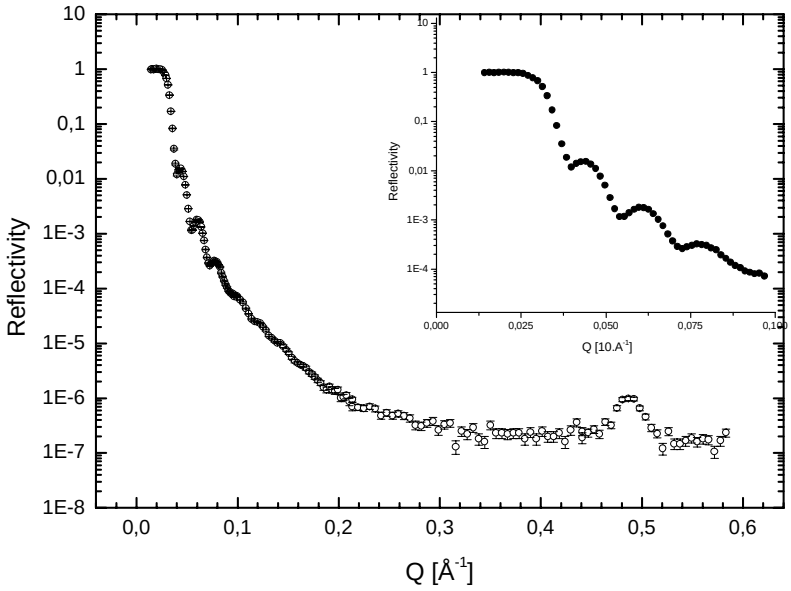

Figure 27. X-ray reflection measurement of 30 nm ZnPc (measured with QCDC) on silicon substrate. Calculations show 36 nm ZnPc layer thickness. The peak with maximum at 0,48 on the Q/Å^{-1} axis corresponds to a layer with thickness 1,3 nm. This can be interpreted as ZnPc molecular sub-layer structure in the main layer

The figure shows a well defined, cascade-like peak structure, where the peaks have a gradually fading intensity. The distance between two peak maxima allows to calculate the layer thickness ($d = \frac{\pi}{\Delta Q}$ [33]), which in this case is 36 nm. So 6 nm too much have been evaporated. The figure shows, also a peak with maximum at 0,48 on the Q/Å^{-1} axis. It corresponds to a layer thickness of 1,3 nm. Since the molecule of a ZnPc has a similar size, this can be interpreted as ZnPc molecular sub-layer structure in the main layer. Fitting of the data to a theoretical model revealed the following ZnPc layer configuration (Figure 28).

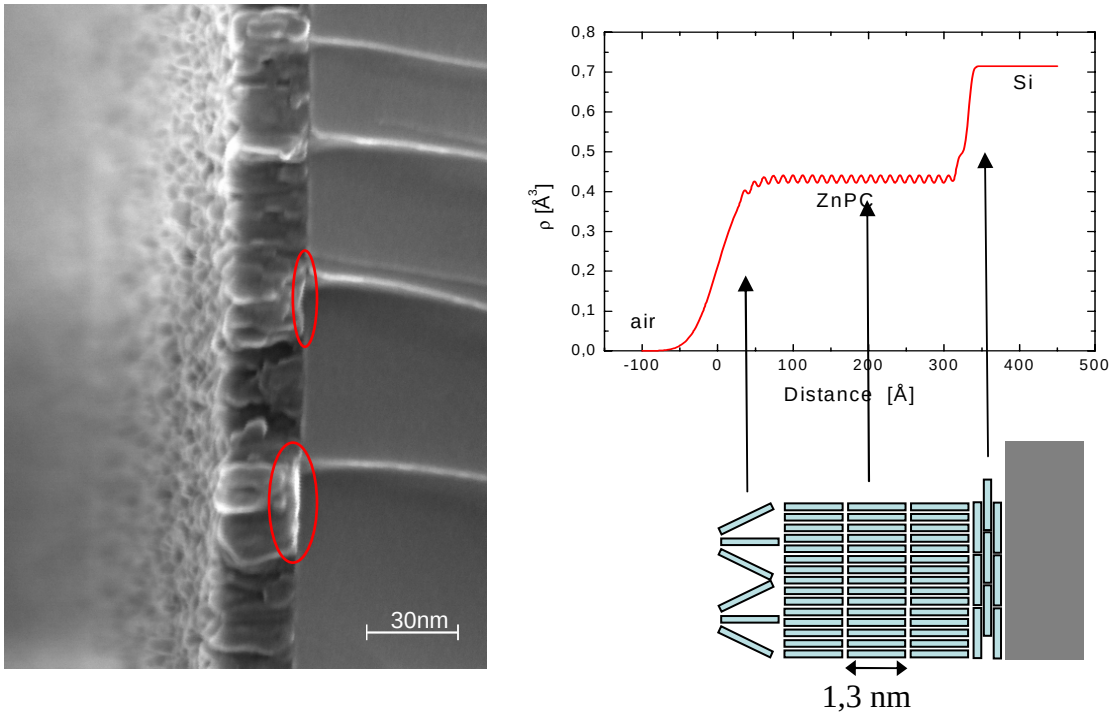

Figure 28. X-ray reflection data fit, layer scheme and an SEM image of a 30 nm ZnPc layer, evaporated on Si (100). The fit reveals 3 different sub-layers. First evaporated nanometers lie horizontally on the Si surface. Then sub-layers with 1,3 nm thickness are evidence for perpendicular to substrate surface molecules. Surface roughness is referred as third layer. The SEM image also shows some regions of ZnPc, near ITO, where some differences to the bulk areas are observed

Figure 28 shows an X-ray reflection data fitted to a multilayer model, layer scheme and an SEM image of a 30 nm ZnPc layer, evaporated on silicon. It should be mentioned here, that the scheme is not absolute and the molecules do not definitely arrange that way. It is only intended to show, that three different sub-layers are discovered. In the model fit the different electron density steps stand for different substances. The slope between Si and ZnPc has a shoulder, near the ZnPc density level, showing a different ordering of this same substance. The model attributes that to the first evaporated nanometers of material, which lie quasi-horizontal on the Si surface. The sub-layers with 1,3 nm thickness are evidence for almost perpendicular to substrate surface ZnPc molecules, since this size is comparable to the size of a single ZnPc molecule. The slope from ZnPc electron density to zero density is attributed to surface roughness and is referred as third layer. The middle of this slope is chosen as zero point, i.e. this is where air and organic material have equal presence.

The SEM image illustrates the ZnPc layer on Si, where some regions, different from the bulk are observed, near ITO. Also the surface roughness, predicted from the model fit, can be seen.

This structural analysis leads to the conclusion, that ZnPc layers consist of molecular sub-layers, with two different molecular orientations and structures contributing to surface roughness. Here it has to be mentioned that this x-ray measurement of ZnPc was made immediately after the evaporation of the organics, thus avoiding any recrystallization and change of surface roughness. A measurement of the same sample a week later showed almost 50% roughness, which resulted in a reflectivity/angle plot, having no peaks at all. This, of course, makes determination of the layer thickness impossible, and is an evidence of rapid recrystallization of the ZnPc even at room temperature.

The x-ray reflection measurement of a 30 nm C60 layer, yielded the following result (Figure 29).

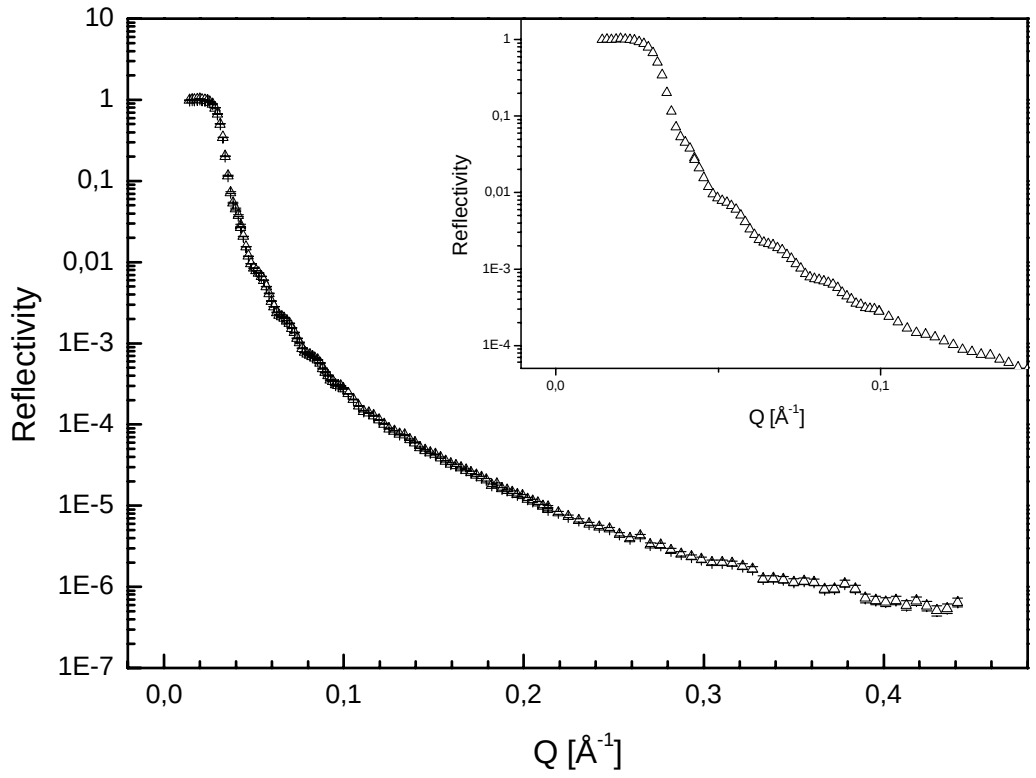

Figure 29 X-ray reflection measurement of 30 nm C_{60} (measured with QCDC) on silicon substrate. Calculations reveal a C_{60} film thickness of 32 nm. High surface roughness influences measurement accuracy

For C_{60} the Bragg reflection oscillations in the R/Q curve are not so well defined, even if that region is zoomed. This is an indication of high roughness, although the sample has been measured directly after evaporation of the organic substance. This result for a C_{60} layer is not unexpected. Literature sources [**50**] show that, during evaporation, after being distributed in a monolayer on the substrate, further C60 molecules start piling up on each other, thus creating clusters and opening free space on the substrate surface. Only after growing big enough, these fullerene clusters cover the surface with a closed layer (Figure 30), consisting of 100-400 nm domains. This explains the behavior observed by us, after evaporating C_{60} on silicon.

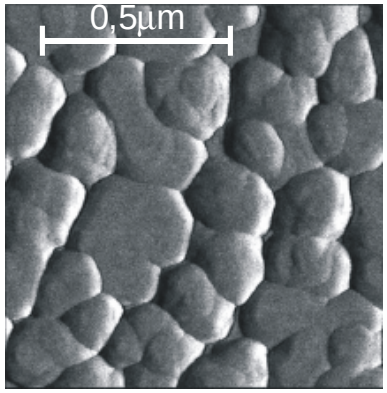

Figure 30. AFM image of 10 nm thick C_{60} film on glass, from [50].

The high surface roughness smudges the peaks and lowers their intensity. Nevertheless the peak positions on the figure can still be located. Calculations show that this fullerene layer has 32 nm thickness. Again a little more than measured by the profilometer calibrated, quartz crystal deposition controllers, but the deviation is not as high as with ZnPc.

For 30 nm BCP (measured with QCDC) the image on Figure 31 was obtained.

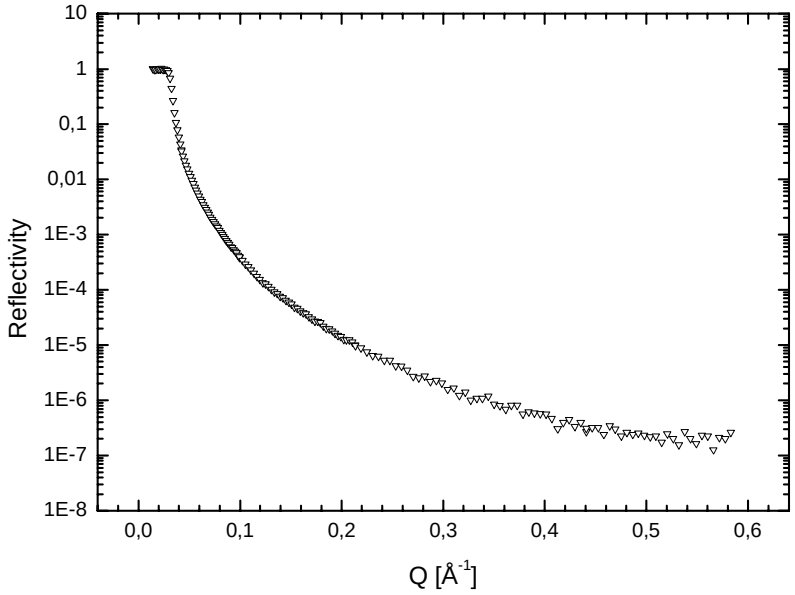

Figure 31. X-ray reflection measurement of 30 nm BCP (measured with QCDC) on silicon substrate. No oscillation peaks for thickness calculation can be obtained, due to high surface roughness, i.e. impossible reflection measurement, due to scattering

The x-ray reflection measurement of BCP showed no distinguishable peaks at all. Here the possible explanations are, that either the very high surface roughness prevents an accurate measurement, or some epitactical growth effect creates organic structures and not a layer, thus leaving the x-ray reflection meaningless.

As a conclusion it can be said that x-ray reflection is a powerful method, concerning layer thickness measurement. Results with angstrom accuracy could be obtained for ZnPc and C_{60} layers, where a well defined layer was present. For BCP the measurement yielded a result which did not allow layer thickness calculation, due to sample incompatibility with the method.

3.4.3 Ellipsometry[4]

For layer thickness determination with ellipsometry, three samples were prepared – ZnPc, C_{60} and BCP, each 100 nm (measured with QCDC). The measurement has been

[4] Ellipsometry measurements conducted at TU Chemnitz

conducted at three angles for each sample: 65°, 70° and 75°, in the range between 0,73 eV and 5 eV. For sensitivity enhancement an autoretarder has been used. The results of the measurement of the layer thicknesses for the three samples are shown in Table 3. It has to be mentioned, that the measurement for ZnPc had to be repeated with fresh samples in order to obtain a reasonable value. First measurement was made on an aged sample, which showed a thickness of 51±48 nm and a roughness of 68±49 nm. Obviously, with this high roughness, our assumption for recristalization of this substance at room temperature is confirmed. The formed crystals make the surface so uneven, that half of the layer thickness is lost into roughness.

Material	Thickness [nm]	Roughness [nm]
ZnPc	113,7±0,4	1,659±0,007
C_{60}	116,8±0,2	3,2±0,3
BCP	82,4±0,7	16±1

Table 3. Layer thicknesses, determined by ellipsometry ZnPc, C60 and BCP. Results are in good agreement with the ones obtained with x-ray reflection. Bathocuproine roughness explains the lack of peaks in the x-ray measurement

In the ellipsometry measurement the result for the roughness of the layers follows the same trend as shown by x-ray. ZnPc with the smallest roughness precedes C_{60}. For the fullerene this value is almost double and clarifies the reason for the worse x-ray reflection peak separation. The 16 nm surface roughness of BCP (≈20%) explains why with x-ray reflection no meaningful layer thickness measurement could be achieved. Simply the method does not function for surfaces, rougher than 10 nm.

The results of the ellipsometry measurement confirm the results from x-ray reflection, that the quartz crystal deposition controllers measure a bit less material, than is actually being evaporated. At this point a correction to the QCDC was made, but the obstacle with unrealistic thickness measurement of the QCDC remains, because of their sensitive nature. Even after small interventions leading to QCDC position change, like maintenance operations inside the UHV chamber, a new absolute thickness calibration has to be done.

As a comparison of the three thickness measurement methods Table 4 can be put together. For ZnPc x-ray shows 20% and ellipsometry shows 14% more than

profilometer measurement. For C_{60} the corresponding values are 7% and 17%, respectively.

Thickness, relative to profilometer	X-ray reflection	Ellipsometry	Profilometer
ZnPc	120%±1,7%	114%±0,4%	100%±10%
C_{60}	107%±1,9%	117%±0,2%	100%±10%
BCP	–	82%±1%	100%±10%

Table 4. Comparison of the film thickness measured by x-ray reflection and ellipsometry, relative to profilometer. Profilometer error is at the lower limit of the real one

As an explanation of the differences it can be said, that on one side the profilometer calibration is inaccurate, but also the density setting in the deposition controller computer might be incorrect. The QCDC measures the layer thickness through mass of deposited material. If the density of the evaporated films is lower than the one of the bulk material, then the layer will be measured thinner than in reality. The mass density of the ZnPc layer can be calculated from the x-ray reflection model fit, using the following formula:

$$\rho_{mass} = \frac{M}{N_A.Z}\rho_{el}$$

where ρ_{mass} is the mass density, M is the substance molar mass, N_A is the Avogadro constant, Z is the number of electrons in one molecule and ρ_{el} is the electron density value from the x-ray reflection model fit. The calculation for ZnPc mass density of the film is 1,41 g/cm^3, compared to a bulk density of 1,65 g/cm^3. This amounts to a 15% difference, roughly as much, as measured with x-ray and ellipsometry.

3.5 Different ITO passivations and their I/V results

There are many known ways to manipulate the surface properties of a TCO – plasma treatment, acid/base treatment, annealing etc [**51**,**52**,56,57]. These treatments usually influence the surface work function of the TCO by modifying the surface chemistry, thus raising or lowering the potential, needed to inject or extract an electron from the TCO electrode [27]. Being able to control and modify the surface electronic properties, makes it possible to fine-tune its parameters for better performance in a PV device. By influencing the surface chemistry, exciton and charge carrier traps could be possibly removed and also a better electrical conductivity through the organic-inorganic interface could be achieved, thus increasing the possible currents which can flow.

In order to find the surface treatment which works for our cells, we have tried several TCO surface chemical modification techniques, each of them including one or more substances tested. The aim of these chemical modifications of the ITO surface is the alignment of the energy bands at the organic-inorganic interface, as well as the variation of the contact resistance. The I/V characteristics of each cell with modified ITO electrode have been measured and presented in the next sections of the current work. Additional measurements and analysis of the chemical TCO treatments will be presented separately in 0, together with the analysis method for clarity and easier result comparison.

3.5.1 Spin coating

The “standard” and mostly used way to modify the surface of an ITO electrode, to be used in a PV device, is the introduction of an additional buffer layer – PEDOT:PSS [**53**]. Through spincoating of this material the whole ITO surface is covered with an extended organic layer having a defined work function.

As a commercial product PEDOT:PSS has a formula which is not very well known to the public. Known is only that it consists of a block-copolymer PEDOT:PSS (Poly-Ethylene DioxyThiophene : Poly-Styrene Sulphonate) with a bad water solubility and polymer-chain length not more than 50-60 units. Thus it comes not as a solution, but as an emulsion in water, sometimes containing some 2-propanole. So, many of its

ingredients are only to be guessed – adhesives and resins, emulsifier agents, inorganic counter-ions like Na^+, etc.

Spin coating allows only limited ways of controlling the deposited layer thickness. Either by varying the emulsion concentration or by controlling the spin coater turning speed one can achieve some well defined surface coverage. Then after applying the PEDOT:PSS, the substrate must be heated for 10 min 100°C in air, to allow the organics to melt and bind the surface in a polymer net. An I/V characteristic of a standard cell whose ITO is covered with PEDOT:PSS can be seen on Figure 32 in comparison with a non PEDOT:PSS cell:

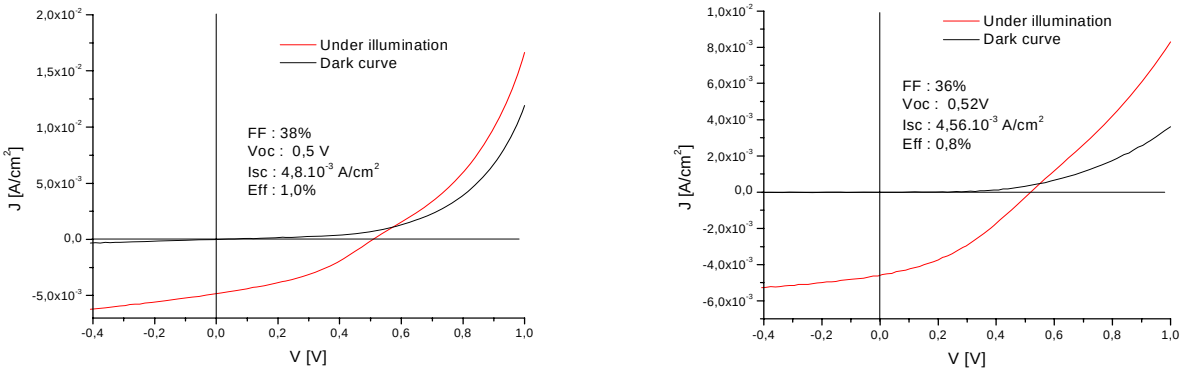

Figure 32. I/V curve of a cell with PEDOT:PSS (left) and without PEDOT:PSS (right)

In the figure it is clearly comparable that a cell with PEDOT:PSS has an improved serial resistance and by the same V_{oc} higher currents are able to flow (J_{sc}). From there the fill factor gets a little higher and the power conversion efficiency of the cell improves. The influence of PEDOT:PSS use is obvious. Chemically designed as a better hole conductor, this layer is also believed to block electrons coming from the bulk and only allow the holes travel to the ITO.

Although PEDOT:PSS improves the overall performance of the cell, it also has drawbacks. Its unknown composition makes it difficult to optimize anything in it except its concentration, so it must be used as delivered. Another drawback of PEDOT:PSS is that the spin coating is a separate process between the substrate washing and vacuum evaporation. An interruption like this could make the industrial production process very complicated and therefore expensive. Further more PEDOT:PSS has a blue colour which means it has an optical absorption. This way it diminishes the quantity of

red light left for absorption in the ZnPc layer. PEDOT:PSS also leads to reproducibility problems due to formulation and quality changes from the supplier. But with all these drawbacks, PEDOT:PSS stays the mostly used TCO treatment for PV devices.

3.5.2 Monolayer sublimation-deposition

With the monolayer sublimation-deposition method we tried to eliminate the cell production step of spin coating and immediately after the wet cleaning procedure proceed in vacuum. There a single layer of 8-OH Quinoline is deposited on the surface of ITO using the already described in (2.6.1) two step procedure. The choice of this specific substance was made from a literature source [26] where it was used as an ITO passivation for OLEDs and gave good results. The ITO surface after the reaction should be covered with a chemically bound organic monolayer, making the transfer of electrons between bulk organics and inorganic TCO easier, and hopefully remove any Schottky barrier or interface defects.

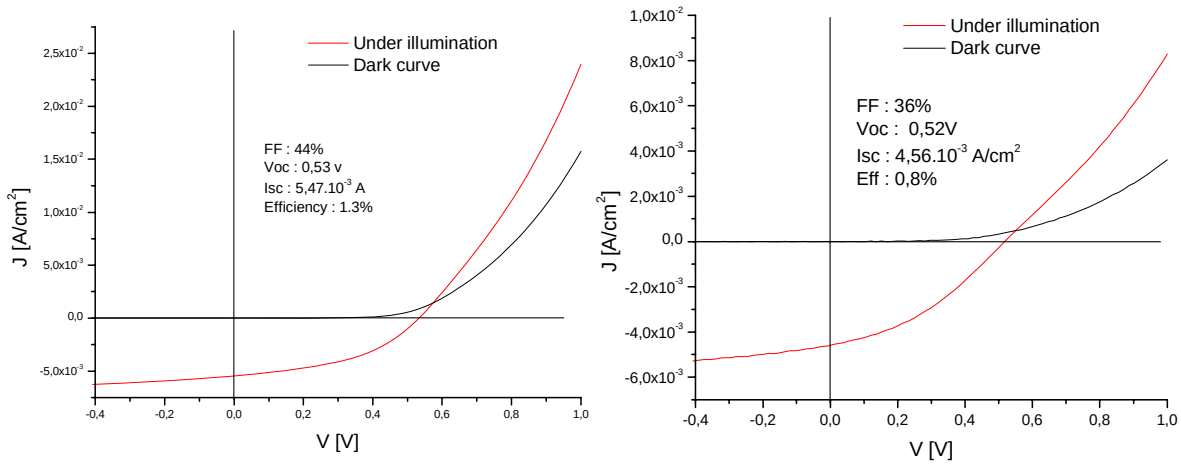

Figure 33. I/V curve of a cell with 8-OH Quinoline passivated ITO (left) and ITO with no treatment (right)

Figure 33 shows a cell with 8-OH Quinoline compared to one with untreated ITO. The organic, although a thin monolayer on the surface [27], helps improve the serial resistance and higher currents are yielded (J_{sc}). The fill factor increases and although V_{oc} stays almost unchanged, the efficiency of the cell is improved.

The possible reason for these improvements is more likely to be the covalently bonded aromatic molecules on the ITO, than a favourable change in the surface work function of the TCO, as we will see in the further analysis of the treatments in 0.

3.5.3 Electro-codeposition

Electro-codeposition of a conducting metal oxide with a dye as a method to produce light absorbing layers is known and has already been used for production of solar cells [**54**]. Although the latter have a low efficiency, the concept of passivating the ITO surface with a thin layer of electro-codeposited ZnO/water-soluble-Pc seems acceptable, mainly because one would expect a coverage preferably at better conducting spots of the TCO, thus creating a conductive nano-wire net. Moreover, the so deposited ZnO is expected to be covered with the water soluble phthalocyanine (tetrasulfophthalocyanine), which happens to be also acidic, thus reacting with the surface of the newly formed ZnO (having an alkaline reaction).

Electro-codeposition was conducted as described in [54] at -1,1 V and 70°C for 15 min, from a solution with concentrations: 0,1M $Zn(NO_3)_2$ and 5.10^{-4}M $CuPc(SO_3H)_4$.

The I/V characteristic of the resulting solar cell is presented on Figure 34.

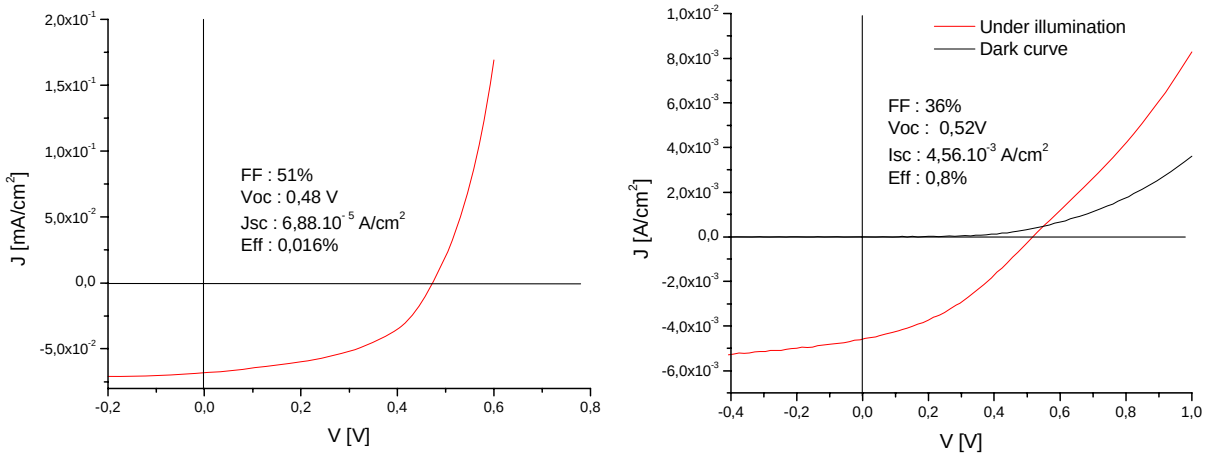

Figure 34. I/V curve of a cell with a thin layer of electro-codeposited ZnO/water-soluble-Pc on the ITO (left; under illumination curve only) and ITO with no treatment (right)

In this cell an interesting effect is to be observed. Having almost unchanged Voc, compared to bare ITO, the fill factor improves as much as with other passivations. Here the low efficiency is due to the very low current flow. Possible reasons include recombination or bad ZnO conductivity, due to lack of dopant (usually Al).

A big drawback of this passivation is that it not only involves an additional procedure in the cell production, but also electricity, which could interfere with a cheap industrial production.

Despite the unexpected outcome, further analysis of this ITO treatment is done in 0 for better understanding of the result.

3.5.4 Dipping

This ITO surface modification technique is a well studied field of TCO science. It has become a favorite because of its simplicity and eventual cost effectiveness. Shortly described, the method consists in dipping the washed and prepared ITO substrates in a solution of the corresponding passivating substance, for a defined time, and then rinsing with plenty of water. This way the passivation becomes a last step in the wet-cleaning procedure. Only the strongly adsorbed species remain on the TCO surface, creating a passivation monolayer. About the coverage one is for sure – it can never be 100%. Anyway, it will be shown that some dip-passivations, even without full coverage of the surface, can provide pretty amazing results in solar cell performance.

3.5.4.1 HCl

Hydrochloric acid was the first substance we tested as a dip-passivation. We tried to influence the work function of the TCO by modifying its surface acidity, as already described in literature [**55**]. ITO was dipped in 1M HCl for 5 min, then washed with plenty of water and dried with nitrogen flow. Thus it was intended to create a surface dipole, charging the inner ITO surface positive and the outer surface negative [**56**]. This would change the surface work function and stimulate electron injection from the TCO electrode into the organic.

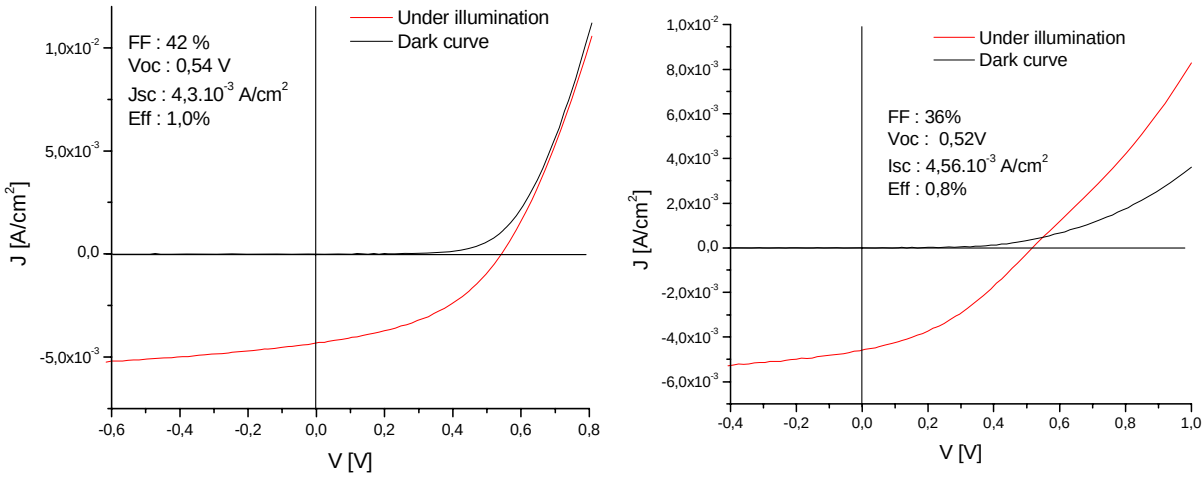

Figure 35. I/V curve of a cell with HCl passivated ITO (left) and ITO with no treatment (right)

On Figure 35 a solar cell, whose ITO was treated with HCl can be compared to a cell with untreated TCO. V_{oc} of both cells shows a minor difference, which can be neglected. As can also be seen from the figure, a higher V_{oc} does not definitely mean a higher short circuit current. An obvious improvement in the serial resistance is observed in the voltage region above V_{oc} for the cell with HCl treated ITO. This improves its fill factor and is the reason of the efficiency increase.

An XPS study of HCl treated ITO substrates showed no presence of Cl^- on the surface though [59]. This led to the conclusion that a strong acid like HCl does not get adsorbed on the surface but only etches the substrate, so a really clean surface is obtained. It is possible that a protonation of the surface occurs, but the effect on cell performance is not that big. That is why we looked for some weaker acid molecule which would get attached to the ITO.

3.5.4.2 H_3PO_4

A surface dipole created by chemi-sorbed acid molecules on the surface of TCOs change their work function [**56**,**57**]. From electrostatics it is also known that a dipole moment equals the charge times the distance between charge centers: $\vec{\mu} = q.\vec{r}$. That is

why phosphoric acid was an apparent choice for an ITO passivation. Phosphate anion has a diameter of 0,26 nm [**58**] (2,6 times bigger than the 0,099 nm ionic radii of chlorine anion) and can have a charge from -1 in dihydrogenphosphate to -3 in phosphate, which could generate a serious dipole on the ITO surface.

Better sticking to metal oxides [**59**] than HCl makes it the perfect surface work function modifying agent. 1M H_3PO_4 treatment of ITO for 5 min yields a cell with I/V characteristics, shown on Figure 36 (left).

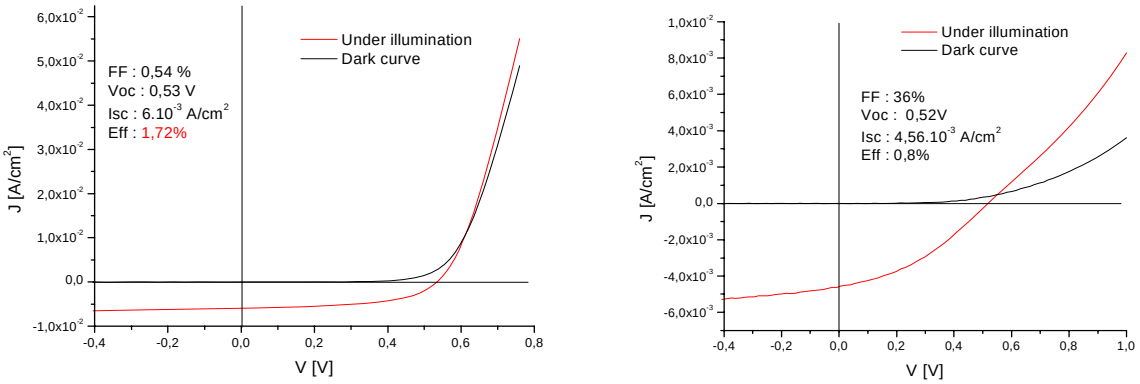

Figure 36. I/V curve of a cell with H_3PO_4 passivated ITO (left) and ITO with no passivation (right)

An exciting record result, concerning the simplicity of the treatment and the method as a whole. In 0 a full surface work function characterization of this ITO passivation is done.

With phosphoric acid passivation a concentration variation was also tried out. The I/V characteristics of solar cells with 10^{-2}M and concentrated (85%) H_3PO_4 passivated ITO are shown on the next figure.

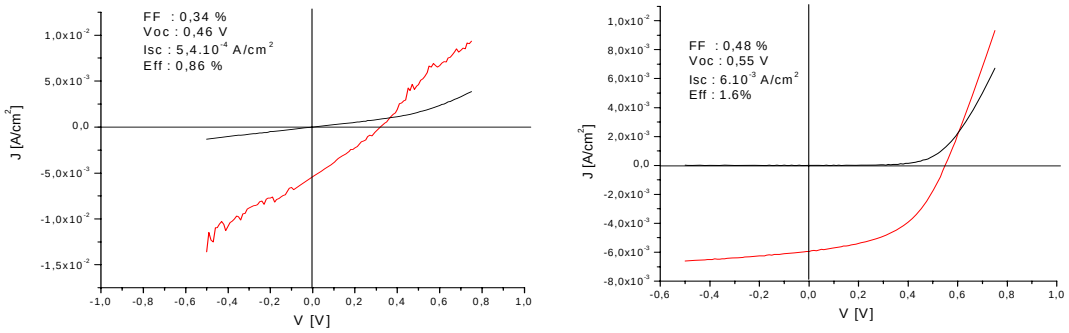

Figure 37. I/V curves of solar cells with 10^{-2}M and ~15M (concentrated 85%) H3PO4 passivated ITO

The cell passivated with 10^{-2}M acid and its measured parameters behave almost as a non-treated ITO cell. On the contrary the cell treated with concentrated acid shows a similar to the 1M H_3PO_4 parameter values. In this case obviously a saturation of the surface is reached even with 1M acid, and higher concentrations do not yield a higher coverage.

3.5.4.3 HIO_4

Per-iodic acid passivation was another try to push the surface work function of ITO even further, by modifying the surface acidity. A per-iodate anion would not have the charge of a phosphate one, but its diameter of 0,33 nm (calculated from literature data [**60**]) is a promise for a big dipole moment, thus a strong change in work function.

In Figure 38 the I/V curve of a cell with HIO_4 treated electrode is shown.

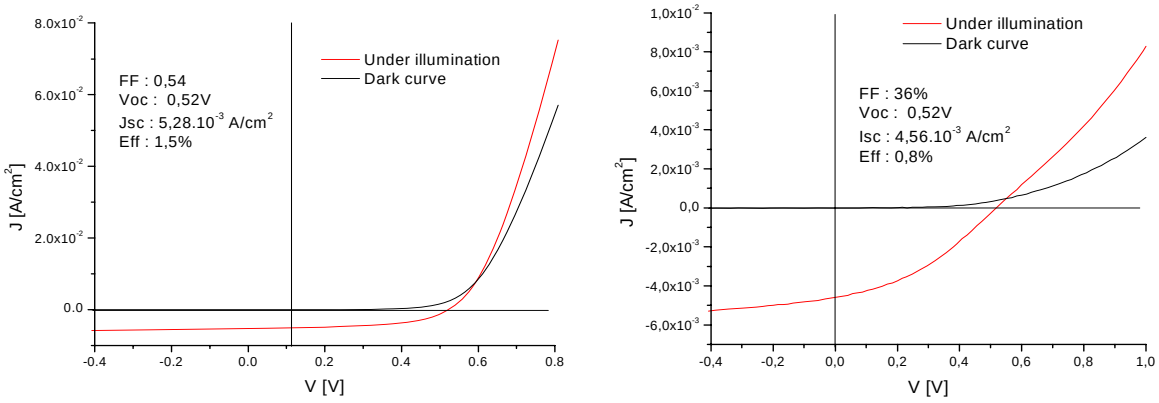

Figure 38. I/V curve of a cell with HIO_4 passivated ITO (left) compared to ITO with no passivation (right)

Per-iodic acid did not yield a record cell, but still a good one. Compared with the 1M phosphoric acid the difference in efficiency comes mainly from less current flow. V_{oc} and FF are about the same. If we compare the serial and parallel resistances (R_s and R_p are described in 2.8) of the non-passivated, H_3PO_4 and HIO_4 cells (Table 5) also other differences are found:

ITO passivation	none	H_3PO_4	HIO_4
R_s [Ω.cm^2]	63,2 ± 0,8	3,06 ± 0,025	2,82 ± 0,039
R_p [Ω.cm^2]	709 ± 29	671 ± 12	704 ± 13

Table 5. Non statistical comparison of Rs and Rp for cells with untreated and H_3PO_4, HIO_4 passivated ITO. Values are calculated from I/V curve fits

The parallel resistance is more or less in the same range for all three samples. The passivation influences much stronger the series resistance. Apparently a big part of the series resistance of the cell comes from the ITO-organic interface. Table 5 is a proof that acid passivation improves the contact between ITO and organics, although the measurement in the first quadrant, during the I/V characterization, is not the extraction of charges from the cell, but their injection. The increase in cell efficiency shows that this improved resistance also influences the cell performance.

3.5.4.4 NH_3

Literature sources [56,57] show that basic treatments of the TCO electrode decrease its work function. This should be critical for the solar cell performance. To obtain better understanding of the TCO work function influence on the solar cell, 1M ammonia solution was tried as a passivation, to observe how a basic treatment would manipulate the cell properties. The I/V characteristic of such a cell did not look like a diode curve at all, so it will not be presented here. The solar cell had practically no photocurrent and efficiency.

3.5.5 Further analysis of ITO passivations

In this chapter a comparative analysis of three differently passivated ITO types will be made. PEDOT:PSS, H_3PO_4 and HIO_4 treated ITO will be compared to untreated ITO. Some additional measurements on ITO passivated with 8-OH Quinoline, co-electrodeposited ZnO/soluble Pc and HCl will be shown. In the search for a better passivation, the advantages of each single treatment have to be considered and the disadvantages overtaken. Only after that, a passivation molecule can be designed, to incorporate all the needed properties and have the advantages of the best treatments.

3.5.5.1 SEM

The electro-codeposition of a conducting metal oxide with a soluble phthalocyanine was unfortunately conducted in the early times of the current research, thus on old samples of 10Ω ITO glass. The surface of this TCO “looked” like the one shown on Figure 39 (upper left).

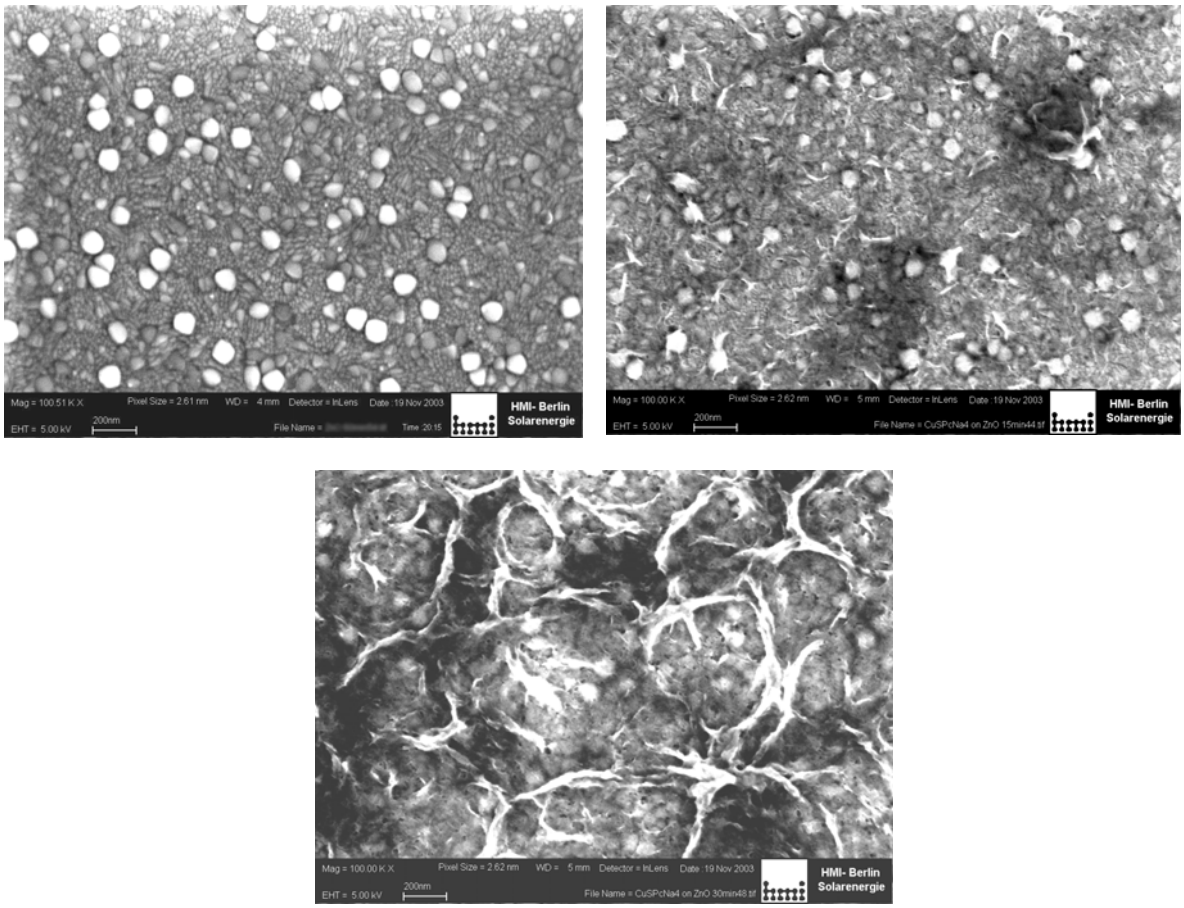

Figure 39. SEM illustration of ITO surface (upper left) covered with co-electrodeposited ZnO/soluble Pc for 15min (upper right) and 30 min (lower image)

Fifteen minutes of electrodeposition with the parameters described in 3.5.3 yielded the surface shown in the upper right of the figure. A ZnO web is created, starting from better conductive places on the surface. There is no homogenous coverage but scattered fibres without preferred direction. The I/V characteristic of a cell produced on such a substrate (Figure 34) showed almost no efficiency due to low photo-current flow, but not only. The explanation here is not simple. The serial resistance of this sample calculated from the I/V curve is $52{,}44 \pm 1{,}39\ \Omega.cm^2$, still lower than the one of bare untreated ITO ($63{,}25 \pm 0{,}76\ \Omega.cm^2$). So there must be a second reason for the low current. Possibly the ZnO web created defects where excitons recombine before they get separated. If the recombination would happen to already separated charges, the voltage would not be the same, but lower.

This passivation technique gave us precious information concerning the possibility of creating traps through ITO treatment. This should be avoided in order to get more efficient in light harvesting process.

3.5.5.2 KPFM

With KPFM the topology of ITO, passivated with different treatments was monitored and its work function was measured, space resolved. The work function strongly depends on the treatment applied [56, 57]. As we will see, the homogeneity of the work function distribution is also affected with the passivation applied.

The results from the KPFM study of bare, untreated ITO surface are shown on Figure 40.

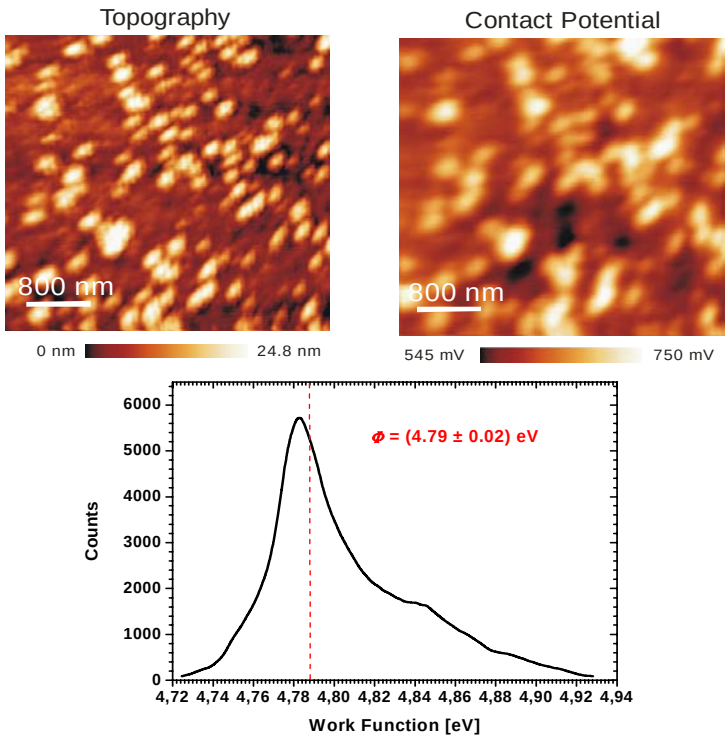

Figure 40. KPFM study of bare, untreated ITO surface[5]. Upper left and right images show the surface topography and contact potential, respectively. Lower graph presents the statistical distribution of the calculated work function, where the mean value is the weighted average

[5] KPFM measurements: Marin Rusu, HMI

The topography image shows a more or less homogenous surface with single peaks of up to 25 nm height. Their origin could be found in the ITO SEM image on Figure 10 and Figure 11. The domain structure of the surface is not completely flat. These domains are situated at a certain angle to the substrate plane, and their highest place could be those peaks in the KPFM image.

When comparing the image of topography and that of the contact potential, one sees certain similarity. Of course the two images are taken on the same area spot. This means that the higher peaks of ITO (shown in a brighter color) correspond to a higher contact potential (also brighter, see legend under images).

This overall inhomogeneous surface shows also inhomogeneity in its contact potential. The mean value for the bare untreated ITO surface work function lies at 4,79±0,02 eV (value is the middle of the half width of the distribution graph). This value lies much higher than the one measured by Nikolas Barreau, mentioned earlier in the current work. The reason is that the first measurement has been done at room temperature without annealing and the measurements of M. Rusu have been conducted after annealing at 130°C in vacuum and cooling to room temperature in order to remove adsorbed water species on the surface, which obviously also changes the work function. At least all the measurements in this KPFM series are conducted the same way, so they are comparable between themselves.

The KPFM illustration of the surface of ITO covered with a monolayer of 8-OH Quinoline (Figure 41) shows completely different electrical properties as compared with untreated ITO.

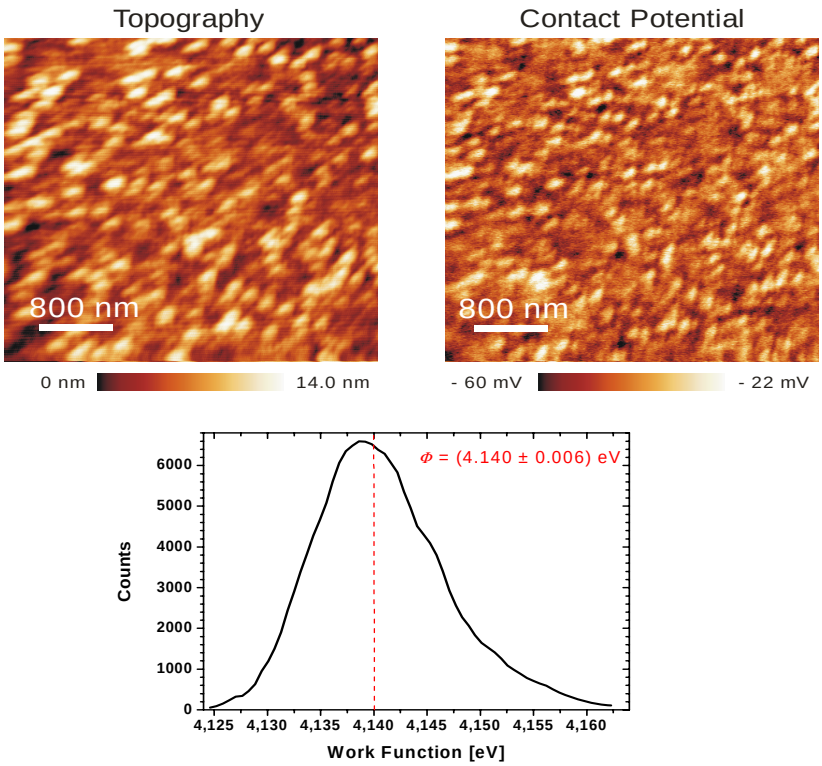

Figure 41. KPFM illustration of the surface of ITO covered with a monolayer of 8-OH Quinoline. Upper left and right images show the surface topography and contact potential, respectively. Lower graph presents the statistical distribution of the work function, where the mean value is the weighted average

Although the topography seems unchanged, the surface work function is in a narrower range compared to untreated ITO. Obviously the covering of ITO with a single, well defined chemical substance smoothens significantly the electrical properties of the surface.

A surprising result of this study is the work function value. For a cell with efficiency 1,3 % where nothing but the ITO passivation is changed one would expect the TCO work function to lie high above the usual one for bare ITO, because this is usual for the better cells. Here this is not the case. A work function of 4,140±0.006 eV was measured. Lower than any other measured value it is even less than the one for untreated ITO. This is a hint that as an ITO passivation 8-OH Quinoline lowers the absolute value of the surface work function of this TCO.

Used as an electrode for a solar cell it yields a cell who's I/V characteristic was already shown on Figure 33. The parameters, fitted from this curve are as follows: R_s=23,6±0,3 Ω.cm^2 and R_p=471±15 Ω.cm^2. R_s is lowered in comparison with untreated

ITO, but still higher than PEDOT:PSS or the dipping passivations. R_p is surprisingly low compared to the other dippings and even untreated ITO (usually around 700 $\Omega.cm^2$). This is a precedent, since it is the only passivation that changed R_p of a cell to such extent (> ≈30 %).

In our scientific discussions there were different opinions concerning the reason for this cell's efficient performance regardless the low work function of the TCO electrode. The dipole created on a surface passivated this way is a weak one, because of the lack of actual charges. Apparently the covalent bond to the ITO surface is responsible for the good connection between the inorganic electrode and the organics. A schematic illustration of an adsorbed/chemi-sorbed acid passivation compared to a covalently bound passivation is shown on Figure 42.

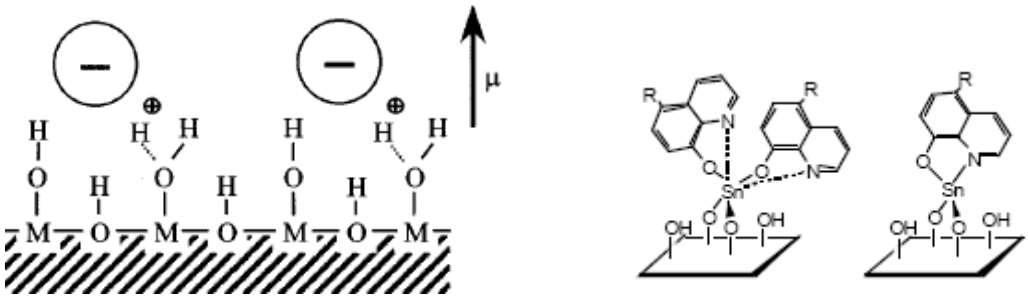

Figure 42. Two different ways of TCO monolayer passivation. "Weak acid" adsorbed on TCO surface (left) [56] and covalently bound 8-OH Quinoline on TCO surface (right) [26]

A strong surface dipole is created only with the adsorption of charged particles (acids/bases). It should ease the charge transfer the following way (Figure 43):

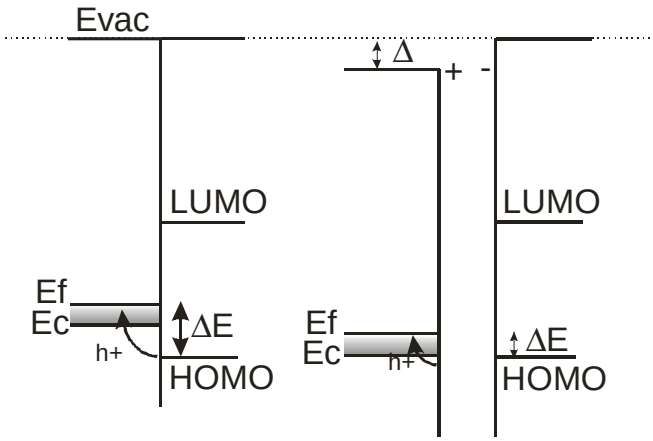

Figure 43. (left) Energy level diagram of the ITO/organic interface. The energy gap between the vacuum and Fermi levels represents the ITO work function. ΔE represents the thermodynamic barrier to hole extraction. (right) Producing a dipole on ITO surface shifts the energy levels of ITO by Δ, increasing ITO work function and lowering the barrier to hole injection.

Holes extracted from the HOMO ZnPc to the E_{Fermi} of ITO need to pass the barrier ΔE. By creating a dipole on the TCO surface, the work function of ITO increases and the thermodynamic barrier for the holes is lowered, thus easing their way to the TCO, through the forbidden zone under the conduction band of ITO. An example of this phenomenon is illustrated on Figure 44 for phosphoric acid passivated ITO.

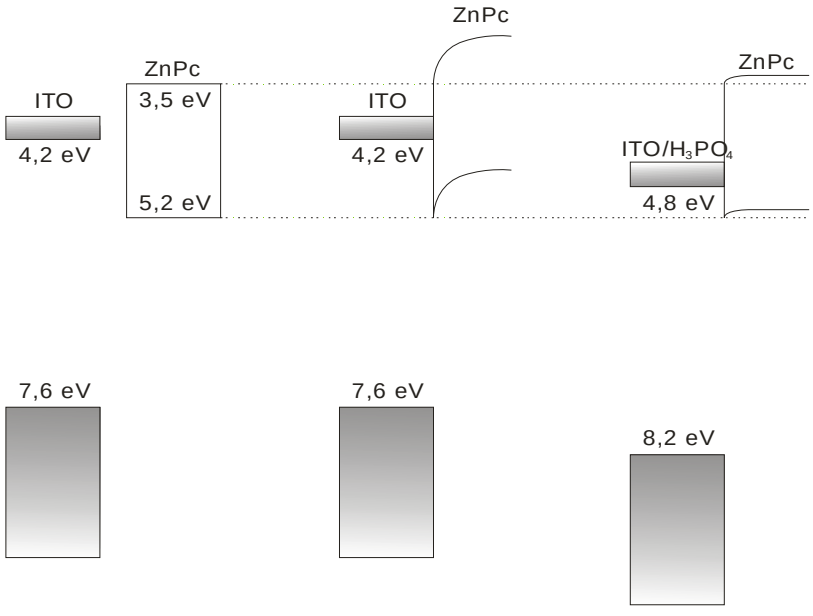

Figure 44. Energy band diagram, showing three possible relations between ITO and ZnPc. Left is shown the case when the two layers are not in contact. The middle case illustrates the ZnPc energy levels upon contact. On the right, an ITO with modified energy levels (H_3PO_4) is shown in contact with ZnPc. It can easily be seen that the thermodynamic barrier from the second case is diminished by the passivation

In the illustration three possible cases of energy band alignment are shown. First, ITO and ZnPc are shown as separate layers. The second case shown is the two layers in contact. A big energetic barrier is created, blocking charge transport. In the third case ITO, passivated with H_3PO_4 with higher work function is shown in contact with ZnPc. There the thermodynamic barrier is much lower, allowing also charge carriers with less energy through.

For a covalently bound passivation this can not be the case. The lack of a real dipole is enough to abandon this theory. A possible explanation of the cell improvement in this case is that the organic molecule bound to the inorganic surface creates a bridge for charges, thus eliminating all surface interface defects and allowing high currents to flow with no option for charge carrier recombination. And really, if J_{sc} for such a cell (Figure 33) is compared to J_{sc} of all the other passivations it becomes clear that only the best cells like 1M H_3PO_4 and 1M HIO_4 passivated have their J_{sc} in the same range.

For H_3PO_4 passivated ITO the KPFM snapshot looks a bit different - Figure 45

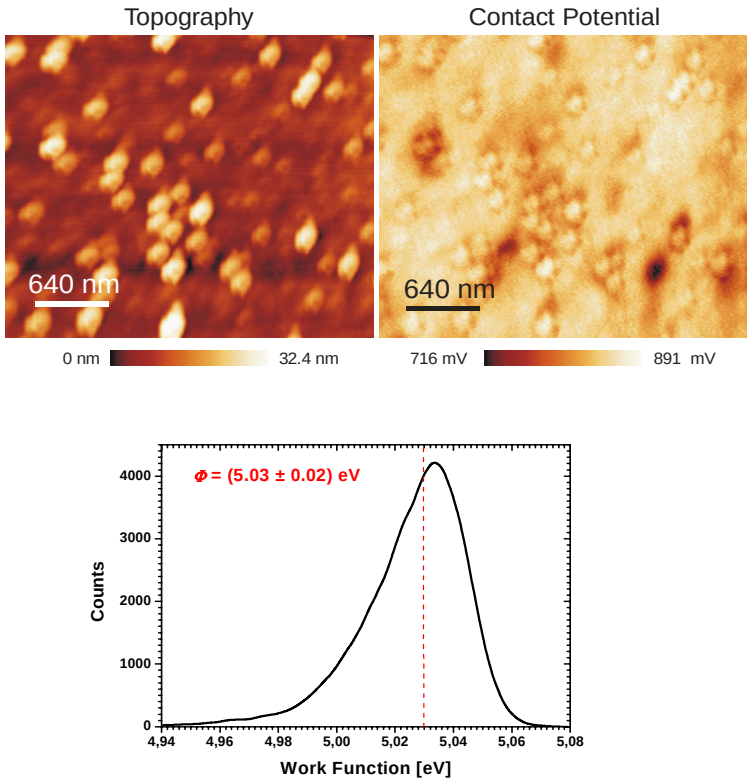

Figure 45. KPFM illustration of the surface of ITO covered with a monolayer of H_3PO_4. Upper left and right images show the surface topography and contact potential, respectively. Lower graph presents the statistical distribution of the work function, where the mean value is the weighted average

Here the topography stays, as expected, unchanged, because a weak acid like phosphoric one does not etch the ITO surface. But this time the contact potential resides in real narrow range, except for some very low potential spot (marked in very dark color on the image). Due to dipole building, the whole surface has almost identical electrical properties. The distribution of the small acid molecule on the surface, as the homogeneity of the contact potential image shows, is amazing. Obviously it reaches even the smallest crack or opening and passivates there also.

The work function of ITO for this passivation, measured with KPFM, is as expected very high: 5 eV we never measured before. And this huge change is induced with such a simple procedure as dipping the sample in a passivating solution and rinsing it thoroughly with water after this. No additional vacuum depositions, no spin coating. And more, this coverage, as proven by XPS (Figure 46) is temperature and vacuum stable up to ≈300°C.

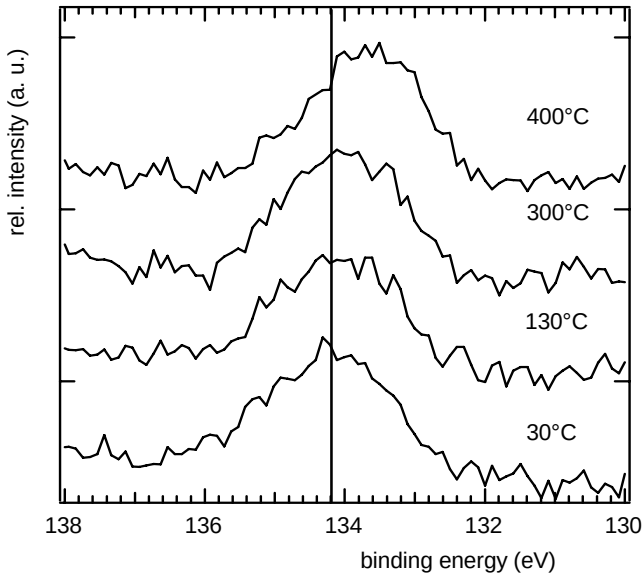

Figure 46. Phosphorus 2p electron peak corresponding to $H_2PO_4^-$ species in a XPS spectrum of H_3PO_4 passivated ITO. Measurement: M. Vogel [59]. Adsorbed species are stable up to 300°C in vacuum, with slight shift to lower energies at higher temperatures (means chemical change)

The phosphorus 2p electron peak corresponding to $H_2PO_4^-$ species, seen in the XPS spectrum of phosphoric acid passivated ITO changes position only after approximately 300°C. For comparison, adsorbed on ITO surface species of per-iodic acid, as measured in [59] are stable, without decomposition, only up to 130°C.

Per-iodic acid (HIO_4) also has a similar behavior to phosphoric acid concerning ITO passivation.

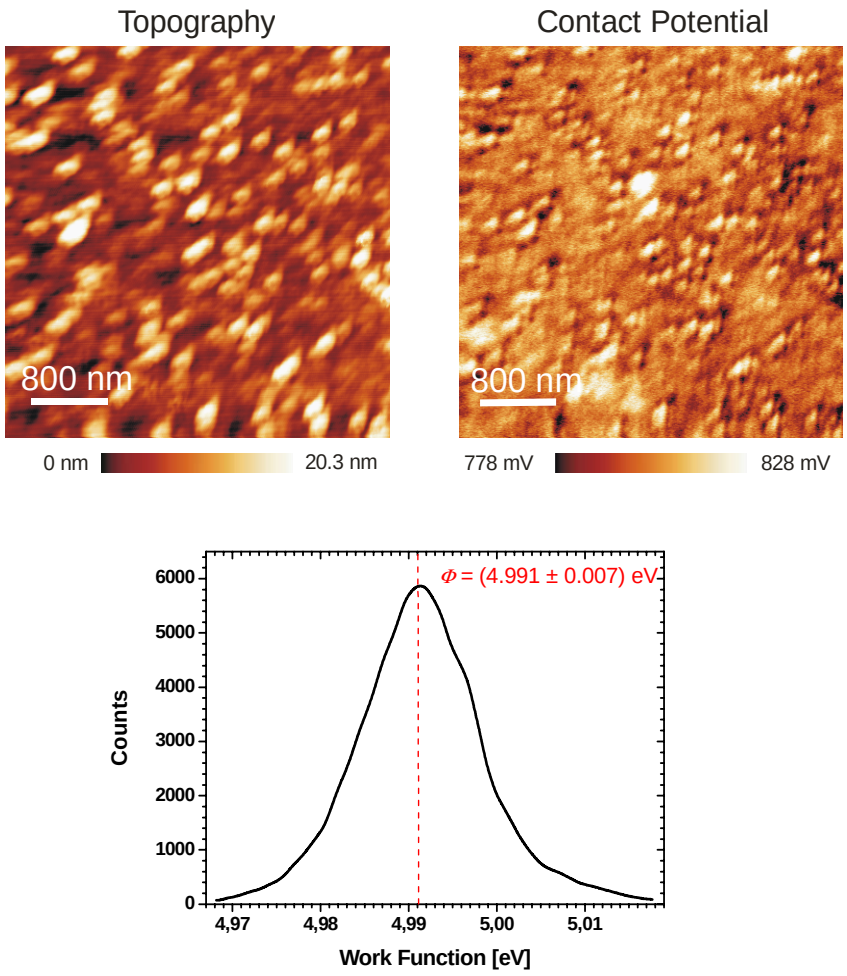

Figure 47. KPFM image of ITO covered with a monolayer of HIO_4. Upper left and right images show the surface topography and contact potential, respectively. Lower graph presents the statistical distribution of the work function and the mean value is the weighted average. Narrow distribution of the surface work function is a hint for surface homogeneity

The surface dipole also keeps surface topology unchanged. Contact potential is again in a narrow range, similar to phosphoric acid. The well defined Gauss distribution of the ITO work function is also to be observed here. The work function value of ≈5 eV is not surprising for this passivation, knowing the I/V characteristic of the cell made with such passivated ITO.

Obviously an optimum has been reached for this kind of passivation and even bigger dipole moment from bigger anion diameter or charge does not affect the work function much more.

3.5.5.3 XPS

A second method we used to measure surface work function and compare the results with KPFM is XPS. The method analyzes the kinetic energy of electrons, emitted from a surface, under irradiation. The binding energy of the electrons in the solid can be calculated using the formula: $E_k = E_X - (E_{bind} + \Phi_{mat})$, where E_k is the kinetic energy of the emitted electron, E_x the energy of the exciting irradiation, E_{bind} the binding energy of the electron and Φ_{mat} is the work function of the material. From the electron binding energy, information on the surrounding of the electron is obtained. Thus, core electron analysis (element and chemical analysis; emission excited with x-rays), or analysis of the outer electron's ionization energies (valence band analysis; emission excited with UV irradiation), can be done.

The XPS values of ITO work function for the different treatments are shown in Table 6, compared with the ones obtained from KPFM.

Work function [eV]						
	Untreated ITO	PEDOT:PSS	8-OH Quinoline	HCl	H_3PO_4	HIO_4
XPS	4,2±0,2	4,6±0,1	3,5±0,1	4,6±0,1	4,8±0,1	4,8±0,1
KPFM	4,3	4,759±0,008	4,140±0,006	–	5,03±0,02	4,991±0,007

Table 6. Surface work function of different treated ITO, measured with XPS[6] and KPFM.

The values measured by XPS and the mean values received from KPFM show a poor agreement. As explained before in 3.5.5.2 the samples are differently pretreated for the two different measurement methods after the passivation. XPS is measured directly after passivation without any further treatment, but samples for KPFM had to be heated to 130°C and cooled down before the measurement to assure the removal of any surface adsorbed water. That should be the reason for the differences in the measured values.

[6] Measurement: M. Vogel [59]

More important in our case, is that the results for both methods are arranged in the same order so they are comparable in terms of ranking.

3.5.6 Short review and estimation of the passivations

In the previous chapters it was made clear that the acid passivations have reached an optimum (H_3PO_4) and further increase of the dipole moment (HIO_4 for example) of the dipole created on the ITO surface contributes almost nothing to the work function raise and to the cell efficiency.

It was also shown that an organic passivation of ITO (8-OH Quinoline) could improve the current flow to the TCO electrode and exclude recombination on traps situated on the TCO surface.

A water soluble passivation could be good enough to substitute PEDOT:PSS – a commercial mixture with little known parameters.

A passivation which shifts the work function of ITO in the desired for solar cells direction should be acidous and not basic.

The ITO treatment should not create, but eliminate TCO surface recombination sites, thus promoting undisturbed charge transfer on the organic-inorganic interface in the solar cell.

If we order the tested passivations in incrementing order of different TCO and cell parameters the following rows can be listed:

- Efficiency:

  ITO<PEDOT:PSS<8-OH Quinoline<Acids
- ITO work function:

  8-OH Quinoline<ITO<PEDOT:PSS<Acids
- Short circuit current:

  ITO<PEDOT:PSS<8-OH Quinoline<Acids

Obviously organic and acid passivation do the biggest favor to the organic solar cell, built on an ITO electrode.

3.6 ZnPc4P – a chemically engineered passivation material

In the search for a state-of-the-art passivation material many simple substances were tested and their efficiency for solar cell production analyzed. Summarizing our studies yielded several properties, that a material should possess, in order to serve as a high-end TCO passivation for solar cells. These properties include:

- Organic compound, with conjugated double bonds in the molecule, in order to achieve a good contact with the first organic layer of the cell, by possible π-orbital overlapping;
- Anionic (acidic). After chemisorption on the surface a dipole will be created, thus shifting the TCO work function to higher absolute values;
- Its acid group(s) should possibly be phosphoric, because of their better sticking to the surface and high stability of the chemisorbed species (proved in 3.5.5.2);
- Water solubility, the easiest way to passivate the TCO electrode and the most cost effective treatment is the dipping procedure

The modification of the surface of the TCO contact also influences the way, the first organic layer in the solar cell grows. The structure of ZnPc, at least in the first several nanometers, depends on the properties of the substrate (epitaxy). On non-polar surfaces ZnPc lays its molecules horizontally, parallel to the surface. On highly polar media the molecules tend to be deposited almost perpendicular to the surface [**61**].

ZnPc, itself possesses some interesting architectural properties. As sketched in Figure 48, ZnPc molecule has anisotropic conductivity 3:1, and its better conductivity is in the direction perpendicular to its molecular plane [62].

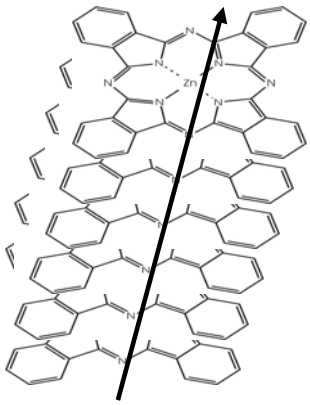

Figure 48. Electrical conductivity axis of the ZnPc molecule and molecular crystal

Also known is that ZnPc crystals consist of slightly shifted in one direction, stacked-overlapping molecules [**62**]. Evaporated on polar surfaces as TCOs, ZnPc creates its crystals parallel to the surface, thus having its molecule plane perpendicular to it [62]. This way the conductivity direction of this layer is almost entirely parallel to the TCO surface. In consequence the current flow is limited by the organic layer resistance. The same is the case with amorphous layers (evaporated on cold substrate) where the conductivity is in all directions, but worse than in crystals, due to the lack of order of the Pc molecules. So if a passivation could help to order the first evaporated layer of this flat molecule parallel to the surface, then all other molecular layers might follow the growth order and the conductivity would be in the right direction - perpendicular to the TCO.

All these requirements for a TCO passivation could be combined in a single molecule, having all the properties needed for a good solar cell. After consideration and revision of all passivation requirements, finally a substance was “born”, incorporating the majority of the properties required (Figure 49).

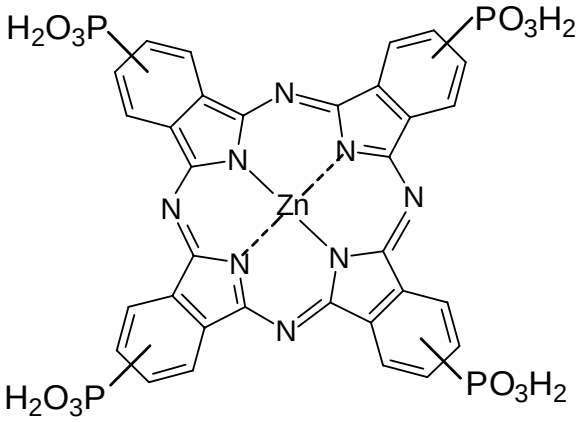

Figure 49. Zinc-Phthalocyaninetetraphosphonic acid (ZnPc4P)

An anionic, water soluble dye molecule, the Zinc-Phthalocyaninetetraphosphonic acid (ZnPc4P) incorporates the phosphate groups and is an organic molecule as a whole. It is similar to ZnPc which ensures the “epitactical” compatibility between passivation and first organic layer.

The synthesis of this substance was conducted as described in 2.6.2. As a passivation it was applied using the dipping procedure, out of a 10^{-4} M aqueous solution. An astonishing fact about this passivation came up after the first passivation test. The ITO substrate turned bluish after only 5 minutes spent in that solution and even huge amounts of distilled water did not wash it away from the surface. This was a hint of the adsorption strength of this substance on the ITO surface.

Of course much could be speculated on the topic why the bluish color could be seen. One possible explanation, is that this phthalocyanine molecule has such a strong light absorption, that even a monolayer can be visible to naked eye. Another possible explanation is the creation of molecule dimers or polymers. As described in [**63**], organic molecules with an acid group, like our substance are capable of creating intermolecular H-bonds (Figure 50).

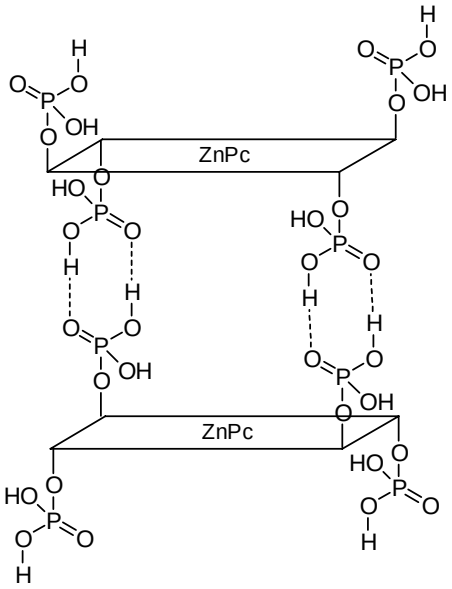

Figure 50. A possible ZnPc4P dimer

So not just a monolayer, but a dimer or even polymer layer could be present on the ITO surface. Although a polymer is very improbable, because the H-bonds are weak ones and by washing with excess of water they would eventually break and substance would get washed away. After all, dimers should only exist in concentrated solutions [**64**].

3.6.1 I/V characterization

After applying the Zinc-Phthalocyaninetetraphosphonic acid as a passivation on ITO a solar cell was produced. Its I/V curve is shown on Figure 51.

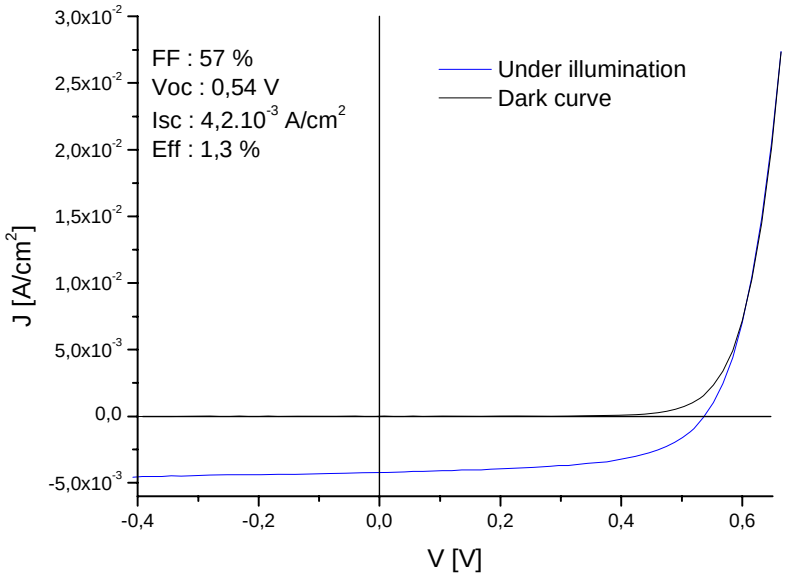

Figure 51. Current voltage characteristic of a solar cell with ZnPc4P passivated ITO

Apart from the not so high efficiency, this cell has the highest fill factor we ever measured. This is due to the improved serial and parallel resistance. R_s: 2,5±0,1 Ω.cm^2 – a hint for an excellent, low barrier contact on the ITO-ZnPc interface. R_p: 1351±62 Ω.cm^2 is almost the double resistance compared to the other passivations. This high parallel resistance stands for extremely low recombination rate of charge carriers at the ITO interface and almost no leakage current [**65**].

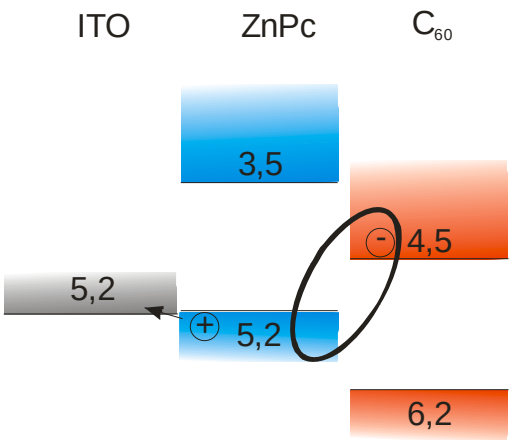

Figure 52. Energy band diagram showing the only possible place in the ZnPc/C_{60} solar cell where recombination could occur (black circle). Having the work function of ITO tuned to 5,2 there remains no forbidden zone for holes under the ITO conduction band, so hole extraction should be the more favored process, than recombination

In Figure 52 the only possible recombination place for the ZnPc/C_{60} solar cells is shown. Tuning the ITO work function to 5,2, the forbidden zone between the conduction band of ITO and the HOMO of ZnPc is no longer a barrier for the hole transport. That is why hole extraction is favored instead of recombination to occur.

Another interesting fact observed in this I/V curve is the perfect matching between the bright and dark measurement in the region above V_{oc}. The reason lies in the electric properties of the ITO. Some TCOs, have almost no charge carriers in the conduction band. When kept in the dark these materials are insulators. As soon as light falls on the electrode charge carriers are excited from the valence to the conduction band and the material turns into a conductor. With ITO the difference in the slope of dark and bright curves (the crossing of the curves) is due exactly to this effect. More charge carriers are created when under illumination, thus the steeper slope. In the case with ZnPc4P as passivation this does not happen, because obviously all possible carriers are already in the conduction band, near the dipole on the electrode surface. So what one observes is matching of the two curves at higher voltages. So the resistance at ITO-ZnPc interface is already not a barrier for transferring even higher currents.

3.6.2 SEM

With SEM we studied the ways of growing the 30 nm ZnPc layer on ITO surface, passivated with ZnPc4P and not passivated. Here it is important to mention that all images of ZnPc on untreated ITO were much harder to focus and to obtain a decent image in comparison to ZnPc4P treated ITO. The reason is that the treated ITO has a much better surface conductivity, thus its interaction with the electrons shot from the SEM electron-gun is much stronger. In SEM better conducting surfaces are easier to see and focus.

The next figure shows a SEM image of the Phthalocyanine layer on untreated ITO.

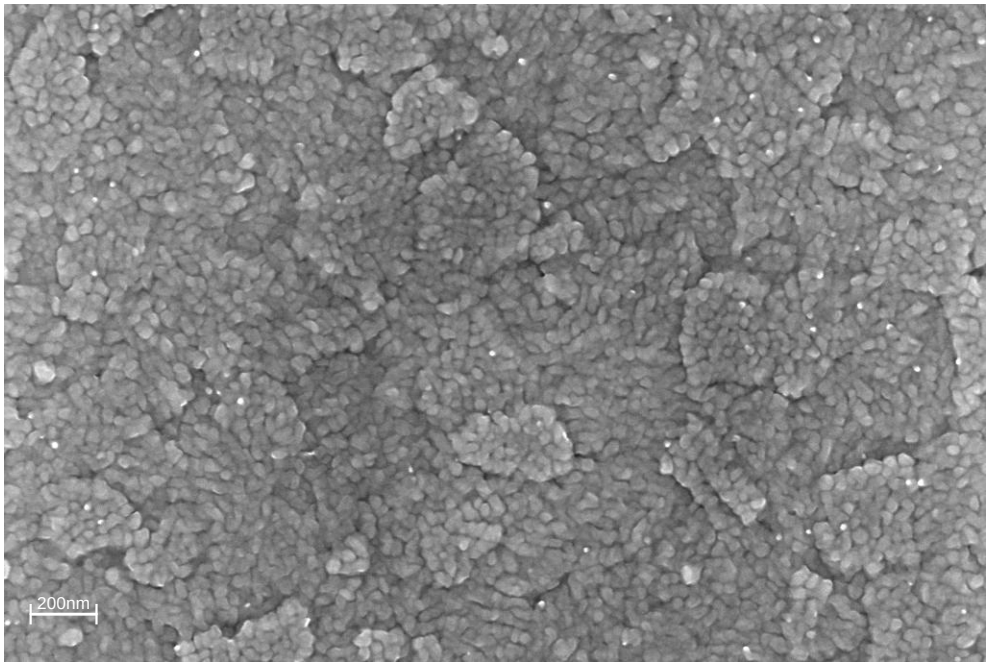

Figure 53. SEM image of 30nm ZnPc on ITO

The original domain structure of ITO is clearly observable. Obviously the layer of ZnPc is thin enough to preserve this structure. On this image the phthalocyanine has some very small “white” spots. These spots are not observed on ITO. So they are some local structure of the organics. Much smaller than the single ITO crystals in a surface domain, these “white” spots have either a very good conductivity and look brighter, or the contrary – they do not conduct but accumulate charge which makes them seem so bright. Usually a surface which accumulates charge drifts in the electron microscope

(glass for example). It is difficult to focus and moves constantly, which makes it impossible to snapshot. Here this was not the case so we assumed the other possibility – highly crystalline and very conductive spots of phthalocyanine.

If we now compare the ZnPc on untreated ITO with the one evaporated on ITO passivated with ZnPc4P, we see the same domain structure of the TCO, but the bright spots of conductive ZnPc have multiplied many times (Figure 54).

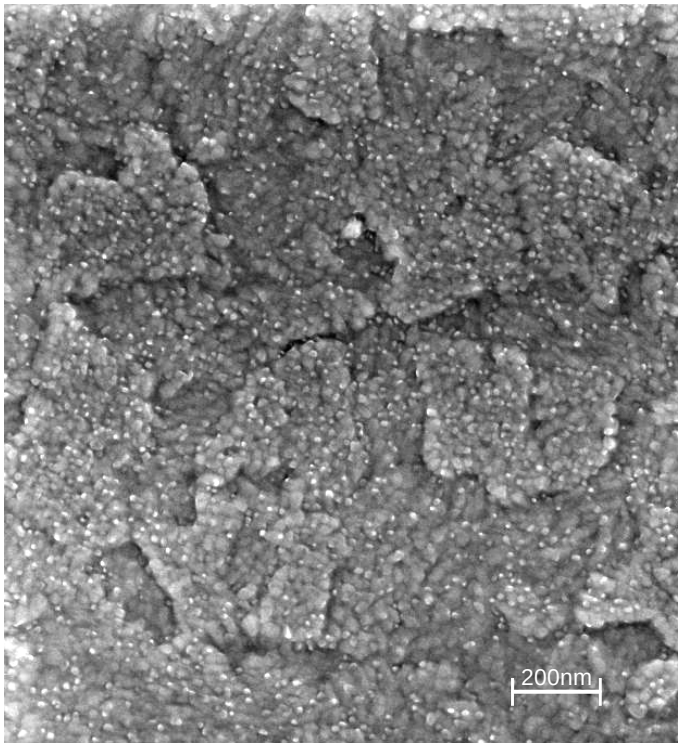

Figure 54. SEM image of 30nm ZnPc on ZnPc4P passivated ITO

If zoomed at some 45° angle to the surface these bright conductive spots look the following way (Figure 55).

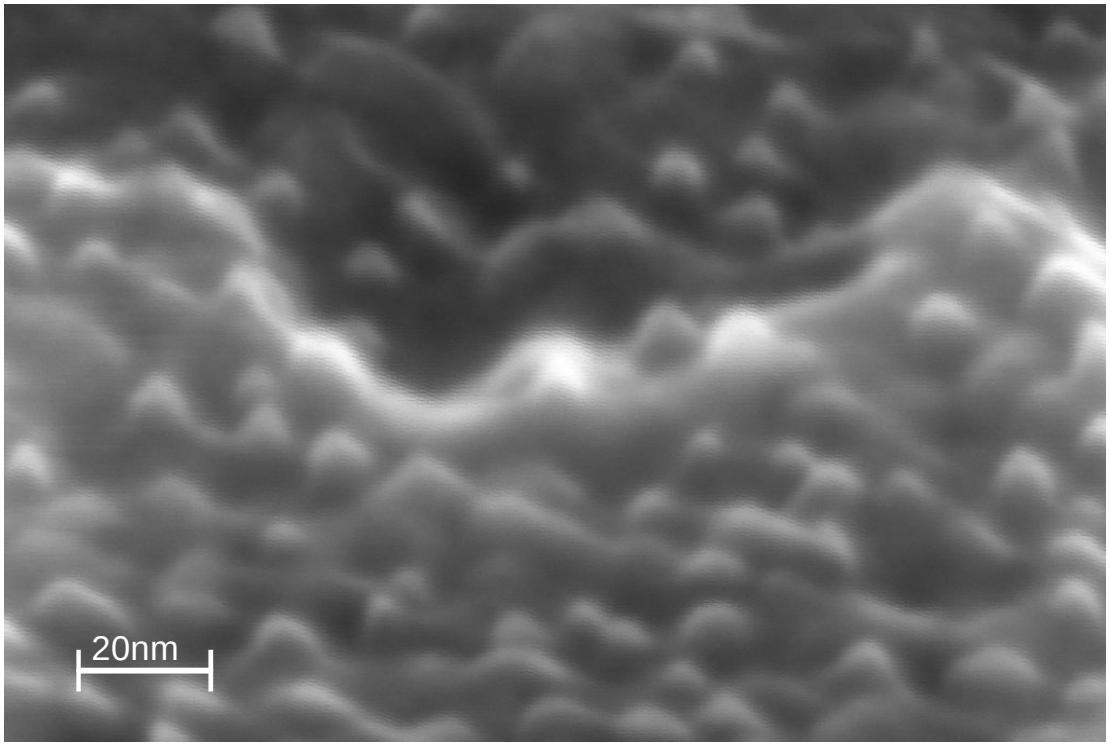

Figure 55. Highly zoomed ZnPc on ZnPc4P passivated ITO

ZnPc4P applied on ITO as passivation helps create multiple highly conductive centers in the layer of evaporated ZnPc. When zoomed in, these conductive centers reveal to be small crystallites in the otherwise amorphous organic layer. So it can be concluded that this passivation manages to cover and prepare the ITO surface on certain spots for probably epitactical crystalline growth. It is well known that evaporated layers of phthalocyanines could be made highly crystalline by increasing the substrate temperature [43]. At room temperature, though, not much can be done about the crystallinity of a vacuum evaporated organic layer. This is where ZnPc4P passivation could help.

To see the effect of this passivation on ZnPc crystallinity, we also conducted a study of evaporating the 30 nm ZnPc layer on ITO at different substrate temperatures. Three layer depositions were carried out on substrates preheated at 60, 90 and 120°C. For those three temperatures both ZnPc4P treated and untreated ITO samples were used. The results are shown for comparison next to each other in two columns in the following Figure 56.

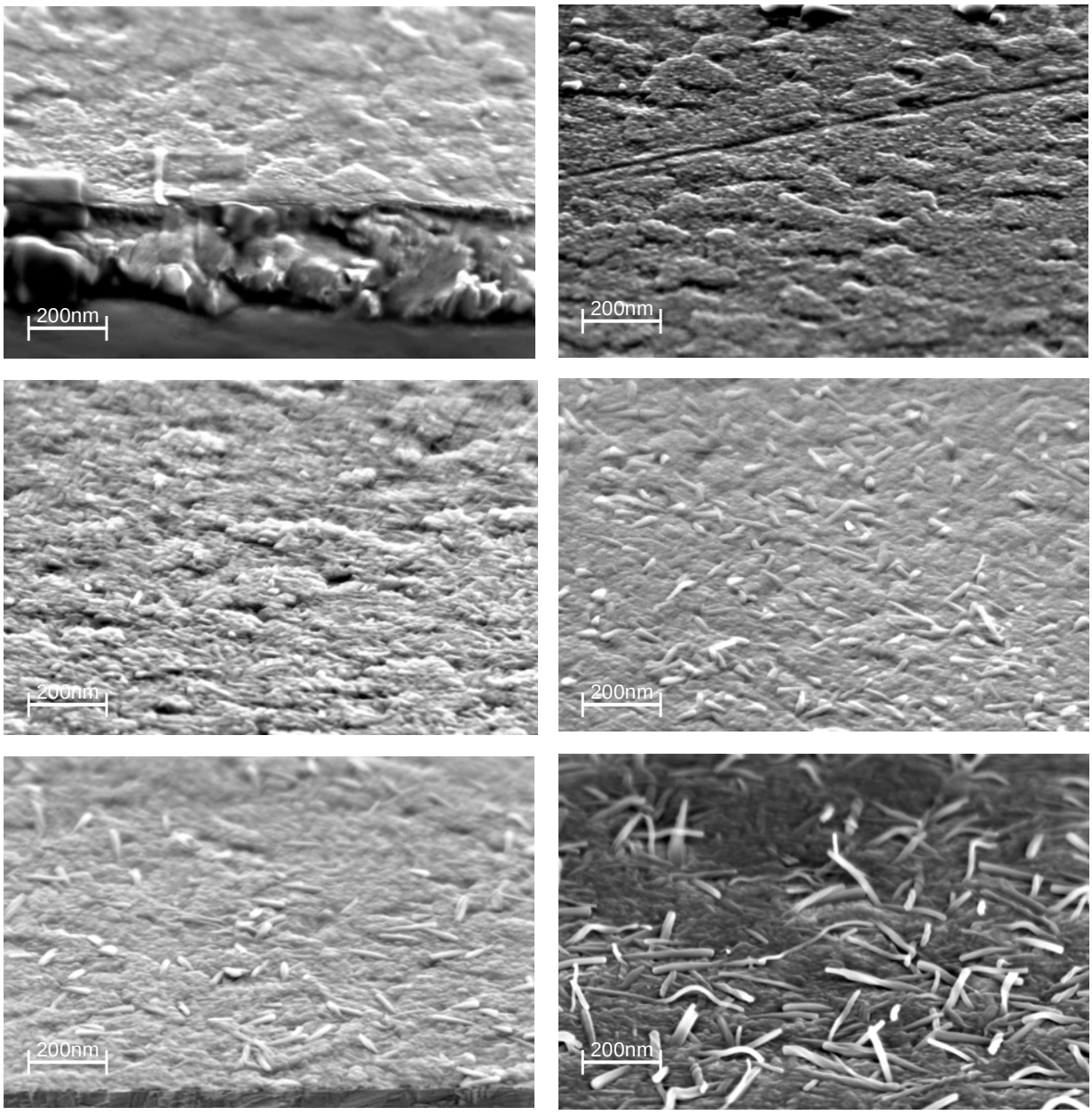

Figure 56. Study of the 30 nm ZnPc layer crystallinity in dependence of substrate temperature and ITO passivation. Left column non-passivated ITO, in descending direcction: 60, 90 and 120°C. Right column ZnPc4P passivated ITO, in descending direction: 60, 90 and 120°C

At 60°C ZnPc on untreated ITO shows the same behavior as at room temperature - homogenous coverage with no particularly expressed structures. Compared to this, at the same temperature ZnPc4P passivated ITO gives a prepared substrate on which the ZnPc creates the small crystallite bumps already known to us from the room temperature deposition.

With 90°C the influence on the crystal growth is stronger. The ZnPc molecules are more mobile, thus creating crystalline bumps even on untreated ITO. For the ZnPc4P treated ITO the image shows clearly observable stick-like crystals, along with the otherwise homogenous coverage.

Heating the untreated ITO to 120°C creates a ZnPc layer, whose topology looks like 60°C ZnPc4P treated surface. In comparison to that the 120°C passivated ITO creates so long crystals, that they already bend, as worm-like structure. Those crystals are also too long to be used in a solar cell, because of shortcut danger.

So to summarize, ZnPc4P as ITO passivation leads to a desired crystallinity in the ZnPc layer of the cell, thus enhancing this layer's electrical conductivity. For the same crystallinity to be obtained on a non-passivated ITO surface, one needs to raise the substrate temperature during evaporation with about 30 degrees higher than for a passivated sample.

3.6.3 KPFM

A work function study of ITO passivated with ZnPc4P was made with KPFM. The results are shown on Figure 57.

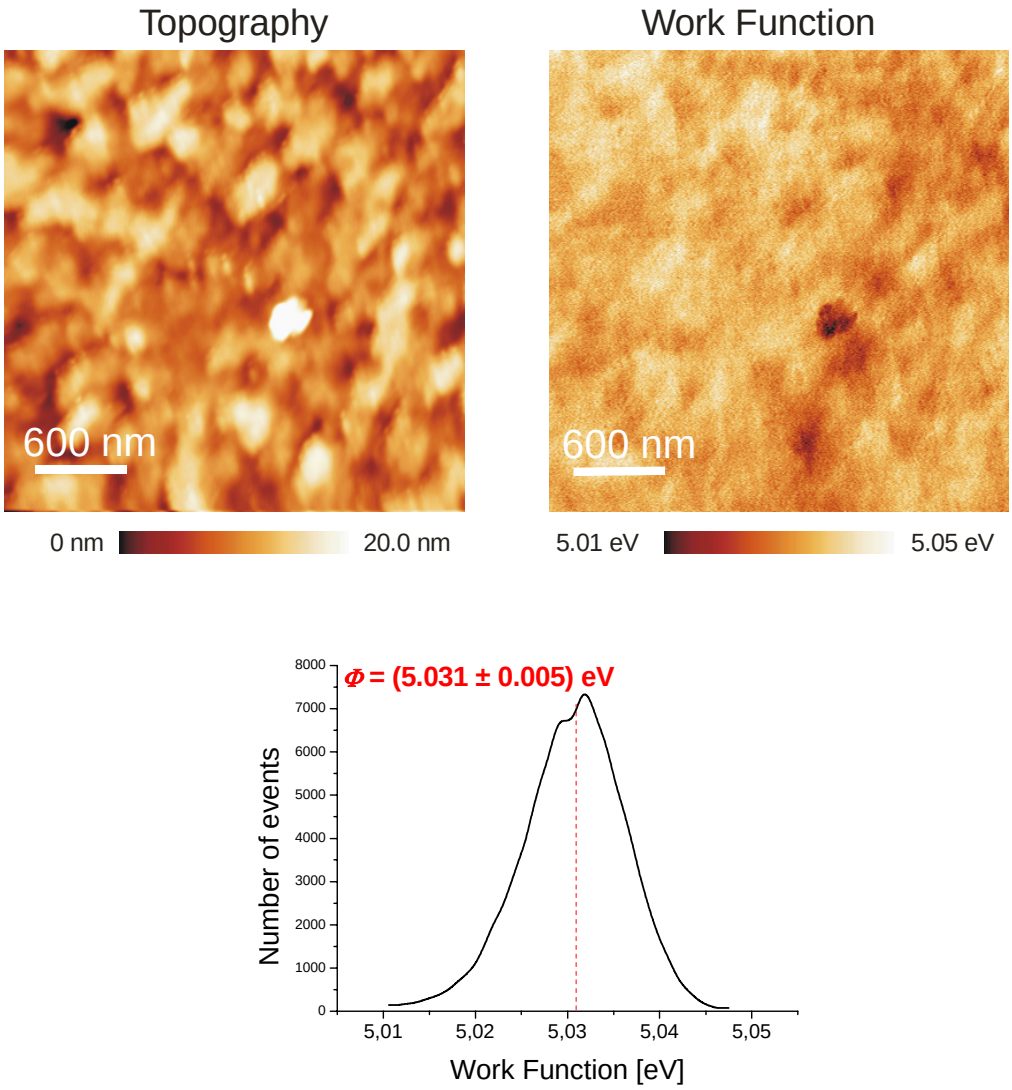

Figure 57. KPFM image of ITO passivated with ZnPc4P. Upper left and right images show the surface topography and work function, respectively. Lower graph presents the statistical distribution of the work function, where the mean value is the weighted average

The topology of ITO stays intact. The work function could not be driven further compared to H_3PO_4, but the value of 5,03 eV is satisfying. Possibly when ZnPc4P dissociates, its first proton the molecule becomes a very weak acid, thus incapable of dissociating a second proton. After all, a strong base as NaOH, for example, is required

to dissociate more protons and get the anion to higher oxidation state. With a weak base like ITO this is not possible. So the charge of the anion stays -1. Eventually this might be also the case with H_3PO_4, which possibly also dissociates only one proton as surface passivation of the weak base ITO. If the two substances create a dipole with the same moment on ITO surface (both dipoles are localized between the phosphoric group and the surface) it is also to expect the same work function value.

3.6.4 XPS

The work function value, measured with XPS, for an ITO sample passivated with ZnPc4P, is 5,2±0,1 eV. The corresponding value for H_3PO_4 (from Table 6) is 4,8 eV. For the KPFM measurement the values for ZnPc4P and H_3PO_4 are the same, but for XPS they differ with 0,4 eV. Having in mind that the error of XPS is 0,1 eV we could not assume that the values measured with XPS are the same even in the error interval. Possibly again the difference comes from the preheating procedure in KPFM.

3.6.5 FTIR of ZnPc4P on TiO_2 P25

In the search of more information on the surface adsorption species created by passivating ITO with ZnPc4P we made an FTIR study. Although we finally obtained a spectrum, we had some difficulties on the way.

The first complication was that we could not measure our ITO samples in transmission, because of the glass substrate (not IR transparent). So we tried attenuated reflection FTIR (ATR-FTIR). With this modification of the method we did not receive any signal from the adsorbed organics. Obviously the adsorbed material quantity is very low, so its interaction with the light was very weak. We also tried transmission FTIR spectroscopy on a single crystal, but there was also no trace of organics in the spectrum.

Finally we decided to try FTIR on a powder sample. It would have enough surface area to adsorb a descent quantity of material and provide a better signal. The only problem we met is that no company had powdered ITO to deliver. So it was decided to work with P25 TiO_2 because of the similarity of the two materials. Although not the

same material, P25 could give us precious information about the adsorbed species on its surface.

So a small quantity of TiO_2 P25 in powder form was stirred in a 10^{-4}M solution of ZnPc4P and centrifuged. Then the liquid decanted and the rest was again dispersed in deionized water to wash the excess of adsorbed material. After a centrifugation, a second wash was performed with deionized water again, and once more centrifuged. The material left was dried in an excicator. Then two KBr pills were prepared, one containing only P25 as a reference and one with ZnPc4P on P25 as a sample. The FTIR spectrum was then measured and compared to one of the clean ZnPc4P material in KBr (Figure 58).

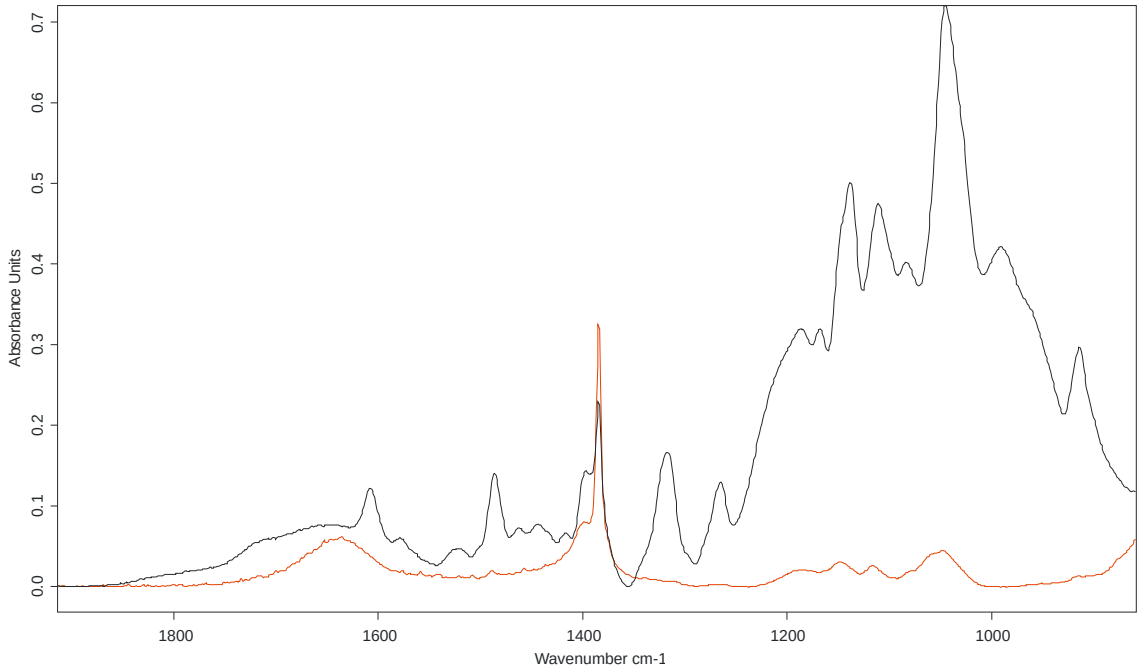

Figure 58. FTIR spectra of ZnPc4P (black) and ZnPc4P on TiO_2 P25 (red), both in KBr. In the spectrum of the passivation, adsorbed on the metal oxide, some of its characteristic peaks are found. No additional information on the adsorption species was obtained, due to weak IR absorption of the adsorbed molecules

The comparison of the adsorbed on TiO_2 $ZnPc_4P$ spectrum to the spectrum of the clean organic material showed, that some characteristic lines match in position in both spectra. This proves that on the metal oxide, even after the two washing steps in the sample preparation, adsorbed ZnPc4P is present. None of the bigger distinguishable characteristic lines has a frequency shift. The most intensive peak in the spectrum of the adsorbed material is the phosphoric group peak (around 1400 cm^{-1}), unlike the original

spectrum of the substance. The intensity increase of this peak could be a clue for ordered structures of the organic substance having the same orientation on the adsorbing surface [**66**,**67**]. Nevertheless the result is unclear and suggests further analysis of the adsorption of this organic molecule on TCO surfaces.

As a conclusion, it can be said that by designing ad applying this new TCO passivation material ZnPc4P, the solar cell parameters, except I_{sc} and therefore η, were improved. Improved were also the cell serial and parallel resistances. It was shown that ITO treated with this material offers impressive substrate for ZnPc crystal growth. The positive contribution to the cell is obvious. Further analysis of this material should be done, to learn more about its TCO surface adsorption species and its part in the interface resistance adjustment. This concept of combining organic and acid passivation in one substance was never reported before, so it is a novel approach. ZnPc4P was never used for a TCO passivation in organic solar cells before.

3.7 Cell up scaling and space resolved I/V measurements

Space resolved I/V measurements on solar cells are helpful to visualize the cell electrical properties, resolved in a way, which shows their distribution on the cell surface. The measurement consists of a focused laser beam, scanning the cell surface pixel by pixel and an I/V measurement unit connected to the cell electrodes, to register the photo-current and voltage. Depending on the electrical properties of the particular spot, being illuminated by the laser, the local current and voltage are registered. Then all the data is displayed in color scale, in dependence of the current strength.

For space resolved I/V measurements our current solar cells are too small. With their 0,032 cm^2 and round form, they are difficult to be found and the laser focused on them. That is why for the needs of space resolved measurements, the cells needed to be up-scaled. Also the form had to change from round to rectangular, because the apparatus scans only rectangular areas. So the sample holder for UHV evaporation and the evaporation masks had to be newly designed and reengineered. The cell encapsulation also had to be completely changed to fit and protect the new, rectangular cell from atmosphere. The blueprints of all newly built parts for the up-scaled solar cells can be seen in **Appendix B**.

With the up-scaled solar cell, which had an area of ≈1cm^2 (11x9 mm), space resolved I/V measurements can now be conducted. An example of a measurement result for a cell with untreated ITO is shown on Figure 59.

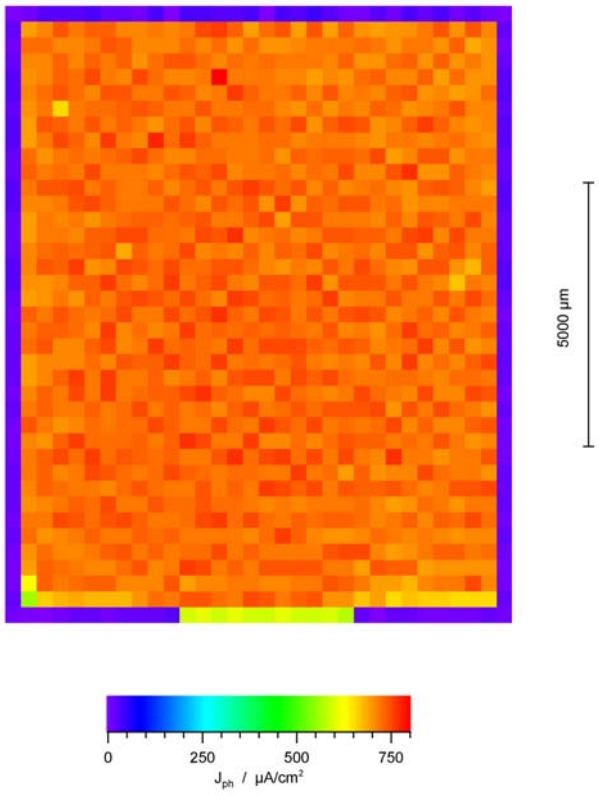

Figure 59. Space resolved I/V measurement of an up-scaled organic solar cell, without ITO passivation or PEDOT:PSS. The blue regions show low currents and the red high current areas. J_{ph} - photocurrent in µA/cm^2

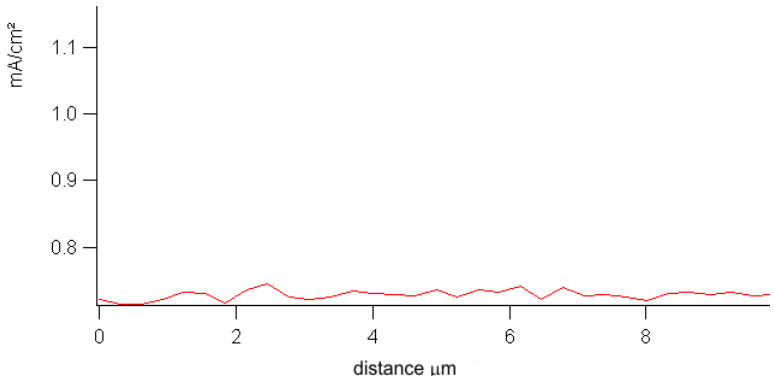

Figure 60. Line scan of the current across the sample.
The even distribution of the values is an indication for a homogenous solar cell

Degradation remains a big problem with space resolved measurements. The measurement itself takes minimum 30-40 minutes, in which time the cell degrades, thus showing a space gradient of the measured current. This is not the real picture which should be observed, but degradation with time creates this effect. That is why the measurement shown on Figure 59 had to be conducted with a very large laser spot, which of course does not allow a fine resolution. Also the scanning speed was set to maximum, so that the degradation effect does not affect the measurement.

On the next Figure 61, the I/V characteristic of an up-scaled cell is shown, produced on H_3PO_4 passivated ITO.

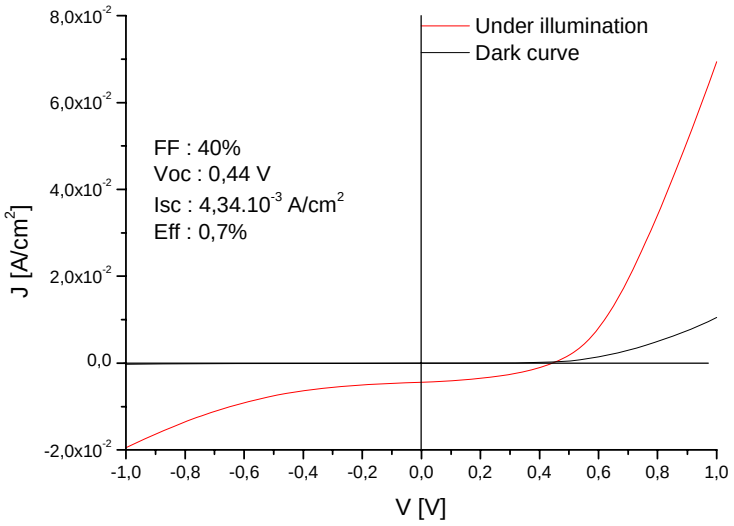

Figure 61. I/V characteristic of an up-scaled (1cm^2) solar cell, on H_3PO_4 passivated ITO. The increasing R_p in the negative voltage region and the low J_{sc} value are an indication for pinholes and increased leakage currents. The efficiency is as expected lower, than for the H_3PO_4 passivated ITO cell with 0,032 cm^2 area

As expected the cell efficiency is lower than the corresponding H_3PO_4 passivated 0,032 cm^2 cell. In the negative voltage region a gradual increasing of the R_p is observed. Together with the low Jsc value for this cell, this is an indication for leakage currents and pinholes through the cell. Possible reasons for this include particle contamination of the TCO surface, high structures of the transparent contact interpenetrating the cell or inhomogeneous cell thickness over this “big” area.